DNA i-motif guided synthesis of a selective telomerase inhibitor

Urmila Saha,[a†] Pratap Paul,[a†] Khushnood Fatma,[a] Raj Paul,[a] Sayantan Pradhan,[a] Zoë Ann Ella Waller,[b] Jyotirmayee Dash[a*]

[a] School of Chemical Sciences, Indian Association for the Cultivation of Science, Jadavpur, Kolkata, India; Email: ocjd@iacs.res.in

[b] School of Pharmacy, University College London, 29-39 Brunswick Square, London, WC1N 1AX, UK.

1.0 General Information

All solvents and reagents were purified by standard techniques; or used as supplied from commercial sources (Sigma-Aldrich Corporation® unless stated otherwise). All the DNA oligonucleotides used for this work were purchased from Sigma-Aldrich. All chemicals and reagents (carbazole, potassium hydroxide, propargyl bromide, 3,6-diiodocarbazole, trimethylamine, $PdCl_2(PPh_3)_2$, CuI, trimethylsilylacetylene, K_2CO_3, 2-bromofluorenone, phenothiazine, sodium hydride, acridone, KO^{t}Bu) were obtained from commercial sources (Sigma-Aldrich Corporation®) and used without further purification. Silica gel F254-coated analytical TLC plates were used for monitoring the reactions. Column chromatography was carried out using silica gel (100−200 mesh). Solvents were removed under low pressure by using a rotary evaporator. ^{1}H and ^{13}C NMR spectra were recorded on either Bruker AVANCE 300 (300 MHz and 75 MHz) or Bruker AVANCE 500 (500 MHz and 125 MHz), or JEOL 400 (400 MHz and 100 MHz) instruments using deuterated solvents as detailed and at ambient probe temperature (300 K). Chemical shifts are reported in parts per million (ppm) and are referred to the residual solvent peak. The following notations are used: singlet (*s*); doublet (*d*); triplet (*t*); quartet (*q*); multiplet (*m*); broad (*br*). Coupling constants are quoted in Hertz and are denoted as J. Mass spectra were recorded on a Micromass® Q-Tof (ESI) spectrometer with 50% methanol solution. The purity of all synthesized compounds was confirmed to be higher than 95% by performing HPLC with a dual pump Shimadzu LC-20 AD system equipped with a 5.0 μm ODS2 reverse phase column (4.6 × 250 mm) using 300 nm detection wavelength. UV−vis spectroscopy was carried out on a double-beam double monochromator spectrophotometer of Jasco V660 (Jasco, Hachioji, Japan) fitted with a thermoelectrically controlled cuvette holder and temperature controller in matched quartz cuvettes of 10 mm path length. Fluorescence studies were performed on a Shimadzu RF-5301PC spectrofluorimeter (Shimadzu, Kyoto, Japan) in fluorescence-free quartz cuvettes of 10 mm path length. A VP-isothermal titration calorimetry (ITC) microcalorimeter (MicroCal, now Malvern, U.K.) was used to perform isothermal titration calorimetry experiments. Both the absorbance and fluorescence spectral titration studies were performed at 298.15 ± 0.5 K. A JASCO J-1500 CD spectrophotometer was used to record the CD spectra.

2.0 Synthesis of DNA coated Au@Fe_3O_4 NPs

Fe_3O_4 nanoparticles were prepared by a co-precipitation method using $FeCl_3$ and $FeCl_2$ in a 1:2 molar ratio under basic conditions. $FeCl_3 \cdot 6H_2O$ (1.0 g) and $FeCl_2 \cdot 4H_2O$ (0.4 g) were dissolved in 100 mL of Milli-Q water under continuous stirring. To this solution, 25% NH_4OH was added dropwise until the pH reached 9.0. The reaction mixture was stirred for 30 minutes at room temperature. After the solution reached pH 9.0, a black precipitate formed, which was isolated by magnetic decantation and thoroughly washed with Milli-Q water. The precipitate was then dissolved in 50 mL of 2 M $HClO_4$, followed by centrifugation to collect the nanoparticles. The resulting pellet was resuspended in 50 mL of Milli-Q water for further use.

Next, an aqueous solution of $HAuCl_4$ (2.26 mL, 2.0 mg mL^{-1}) was mixed with 15.75 mL deionized water and then heated to boiling. Then, 0.75 mL of Fe_3O_4 nanoparticle suspension was added to the reaction mixture followed by the addition of sodium citrate (0.75 ml, 80 mM) with continuous stirring. The solution gradually changed color from brown to burgundy, indicating the formation of gold-coated nanoparticles. The reaction mixture was stirred and heated at 85 °C for 5 minutes. After cooling to room temperature, the solution was sonicated for 5 minutes, and the resulting Au@Fe_3O_4 nanoparticles were collected by magnetic separation, washed thoroughly three times with Milli-Q water, and redispersed for further use. All buffers and solutions were degassed under a nitrogen (N_2) stream to prevent oxidative dimerization of thiolated DNA strands into disulfide-linked dimers. Gold-coated magnetic nanoparticles (Au@Fe_3O_4 NPs) were functionalized with thiolated DNA sequences by mixing 50 μL of Au@Fe_3O_4 dispersion with 50 μL of preannealed 5′-thiol-modified DNA (25 μM).

The thiolated *c-MYC, h-TELO* and *BCL2* G-quadruplex sequences and the thiolated duplex DNA sequence were attached to the nanoparticles in 60 mM Na-cacodylate buffer (pH 7.4) and thiolated *c-MYC, h-TELO* and *BCL2* i-motif sequences were linked to the nanoparticles in 10 mM Na-cacodylate buffer (pH 5.5).

The thiolated G-quadruplex-forming sequences *(c-MYC, h-TELO, and BCL2*) and a thiolated duplex DNA sequence were conjugated to the Au@Fe_3O_4 nanoparticles in 60 mM Na-cacodylate buffer (pH 7.4). The corresponding thiolated i-motif-forming sequences (*c-MYC, h-TELO, and BCL2*) were attached to the nanoparticles in 10 mM Na-cacodylate buffer (pH 5.5). Each functionalization reaction was incubated for 16 hours at room temperature with intermittent stirring. After incubation, the DNA-functionalized nanoparticles were magnetically

separated, thoroughly washed with the respective buffer, and the final volume of each nanoparticle dispersion was adjusted to 100 µL using the same buffer. The HPLC-purified, 5′-thiol-modified DNA oligonucleotides were obtained from Eurofins Genomics. The sequences used in this study are listed below:

c-MYC iM: 5'-[ThiC6]TCCCCACCTTCCCCACCCTCCCCACCCTCCCCA

BCL2 iM: 5'-[ThiC6]CAGCCCCGCTCCCGCCCCCTTCCTCCCGCGCCCGCCCCT

h-TELO iM: 5'-[ThiC6]TTCTTGAATCCCAATCCCAATCCCAATCCCAA

VEGF iM: 5'-[ThiC6]GACCCCGCCCCCGGCCCGCCCCGG

c-MYC G_4: 5'-[ThiC6]TGGGGAGGGTGGGGAGGGTGGGGAAGG

BCL2 G_4: 5'-[ThiC6]AGGGGCGGGCGCGGGAGGAAGGGGGCGGGAGCGGGGCTG

h-TELO G_4: 5'-[ThiC6] TTAGGGTTAGGGTTAGGGTTAGGGTTA

*ds*DNA: 5'-[ThiC6]CAAAAATTTTTGCAAAAATTTTTG

3.0 Synthesis of clickable building blocks

Preparation of 1a:

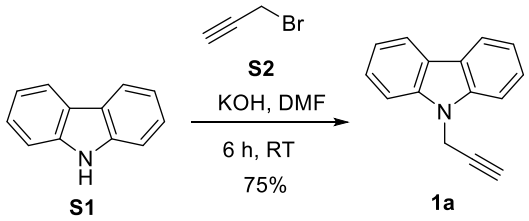

Carbazole **S1** (500 mg, 2.99 mmol) was dissolved in anhydrous DMF (5 mL) and cooled to 0 °C under nitrogen. Potassium hydroxide (224 mg, 3.99 mmol) was added to the solution, and the mixture was stirred for 15 minutes. Subsequently, propargyl bromide **S2** (80% solution in toluene, 0.63 mL, 3.99 mmol) was added dropwise, and the reaction mixture was allowed to stir at room temperature for 6 h. Upon completion (monitored by TLC), the reaction was quenched with water (20 mL), and the mixture was extracted with ethyl acetate (3 × 20 mL). The combined organic layers were washed with brine, dried over anhydrous Na_2SO_4, and concentrated under reduced pressure. The crude residue was purified by column chromatography on silica gel using EtOAc/hexane (2:98) as the eluent to afford the desired product as a white solid (450 mg, 75%). **^{1}H NMR** (300 MHz, Chloroform-*d*) δ 8.24 – 8.20 (m, 2H), 7.64 – 7.58 (m, 2H), 7.56 – 7.52 (m, 2H), 7.44 – 7.38 (m, 2H), 5.00 (d, 2H), 2.33 (t, 1H). **^{13}C{^{1}H} NMR** (75 MHz, Chloroform-*d*) δ 139.9, 125.9, 123.3, 120.5, 119.6, 108.8, 72.3, 32.2. HRMS (ESI) $[M+H]^+$ *m/z*: calculated for $[C_{15}H_{12}N]$ 206.0970, found 206.0972.

Preparation of 1b:

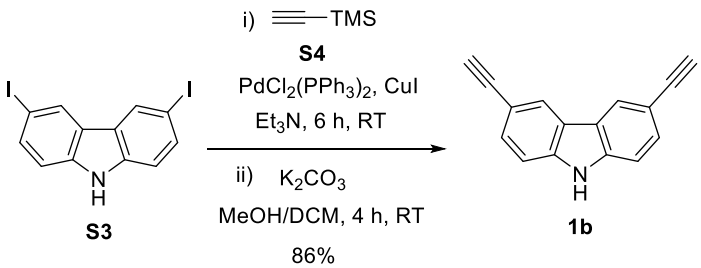

3,6-Diiodocarbazole **S3** (2.0 g, 4.77 mmol) was dissolved in a mixture of anhydrous THF (10 mL) and triethylamine (10 mL) under an argon atmosphere. To this solution, $PdCl_2(PPh_3)_2$ (168 mg, 0.24 mmol) and CuI (45 mg, 0.24 mmol) were added at room temperature, and the mixture was stirred for 30 minutes. Trimethylsilylacetylene **S4** (4.6 mL, 28.64 mmol) was then added dropwise, and the reaction mixture

was stirred under argon for 12 h. After completion, the reaction mixture was concentrated under reduced pressure, washed with brine, and the organic phase was dried over anhydrous Na_2SO_4. The crude product (TMS-protected intermediate) was purified by column chromatography.

The purified intermediate was then stirred with K_2CO_3 (6.6 g, 47.70 mmol) in a methanol–CH_2Cl_2 mixture (1:1, 50 mL) under an argon atmosphere for 4 h to remove the TMS protecting groups. The solvents were removed under reduced pressure, and the residue was washed with brine and dried over Na_2SO_4. Purification of the crude product by column chromatography on silica gel using EtOAc/hexane (15:85) afforded the desired product as a yellow solid (883 mg, 86%). **^{1}H NMR** (300 MHz, Chloroform-*d*) δ 8.23 (s, 1H), 8.21 (dt, J = 1.5, 0.7 Hz, 2H), 7.57 (dd, J = 8.4, 1.5 Hz, 2H), 7.37 (dd, J = 8.4, 0.7 Hz, 2H), 3.08 (s, 2H). **^{13}C{^{1}H} NMR** (101 MHz, Chloroform-*d*) δ 139.8, 130.6, 124.9, 122.9, 113.7, 110.9, 84.7, 75.7. HRMS (ESI) $[M+H]^+$ *m/z*: calculated for $[C_{16}H_{10}N]$ 216.0813, Found 216.0811.

Preparation of 1c:

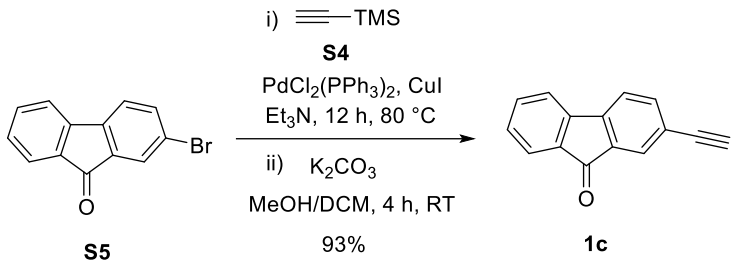

To a 100 mL round bottomed flask, 2-bromofluorenone **S5** (1g, 3.86 mmol), $PdCl_2(PPh_3)_2$ (135 mg, 0.19 mmol) and CuI (37mg, 0.19mmol) were added. The flask was evacuated and back-filled with inert gas (argon) three times to ensure an oxygen-free atmosphere. Then 20 mL dry THF, TMS-acetylene **S4** (1.3 mL, 7.72 mmol) were added.

The reaction mixture was refluxed at 80 °C overnight. After cooling to room temperature, a saturated aqueous NH_4Cl solution was added. The aqueous layer was extracted with dichloromethane (DCM), and the combined organic phases were washed with brine and dried over anhydrous Na_2SO_4. The solvent was removed under reduced pressure. The crude product was purified by column chromatography (hexane as eluent) to afford the TMS-protected alkyne as a yellow solid.

The protected product was then stirred with K_2CO_3 (5.3 g, 38.60 mmol) in a methanol/diethyl ether mixture under an argon atmosphere for 16 h to remove the TMS group. The solvents were evaporated to dryness, and the residue was redissolved in ethyl acetate (EtOAc) and washed with water. The organic phase was separated, washed with brine, dried over Na_2SO_4, and concentrated under reduced pressure to yield the final product as a yellow solid (700 mg, 93%). **^{1}H NMR** (400 MHz, Chloroform-*d*) δ 7.75 (s, 1H), 7.69 – 7.66 (m, 1H), 7.62 – 7.59 (m, 1H), 7.53 – 7.47 (m, 3H), 7.32 (td, J = 7.0, 2.0 Hz, 1H), 3.16 (s, 1H). **^{13}C{^{1}H} NMR** (101 MHz, Chloroform-*d*) δ 193.0, 144.5, 143.9, 138.4, 135.0, 134.5, 134.3, 129.7, 128.0, 124.7, 123.1, 120.9, 120.4, 82., 78.9. HRMS (ESI) $[M+H]^+$ *m/z*: calculated for $[C_{15}H_9O]$ 205.0653, Found 205.0654.

Preparation of 1d:

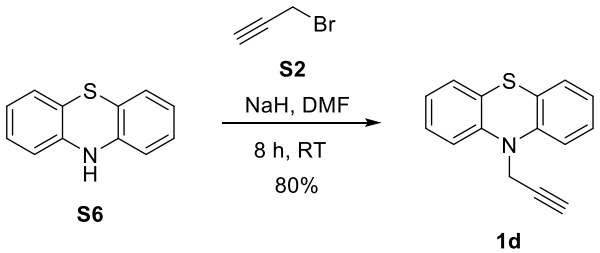

Phenothiazine **S6** (1g, 5.02 mmol) was taken in anhydrous DMF (30 mL) in a dry round-bottom flask under an inert atmosphere. The solution was cooled to 0 °C, and sodium hydride (60% dispersion in mineral oil, 401.5 mg, 10.04 mmol) was added carefully. The reaction mixture was stirred at room temperature for 30 min. Then, propargyl bromide **S2** (80% solution in toluene, 0.76 mL, 10.04 mmol) was added

dropwise, and the reaction mixture was stirred continuously at room temperature for 8 h. After completion, the reaction was quenched with ice-cold water, and the precipitated solid was filtered, washed with water, and dried under vacuum to afford the desired product as a solid (955 mg, 80% yield). **^{1}H NMR** (400 MHz, Chloroform-*d*) δ 7.25 – 7.18 (m, 4H), 7.17 – 7.12 (m, 2H), 7.00 – 6.95 (m, 2H), 4.53 (d, *J* = 2.4 Hz, 2H), 2.47 (t, *J* = 2.4 Hz, 1H). **^{13}C{^{1}H} NMR** (101 MHz, Chloroform-*d*) δ 144.2, 127.5, 127.1, 123.4, 123.1, 114.9, 79.3, 74.5, 38.6. HRMS (ESI) $[M+H]^+$ *m/z*: calculated for $[C_{15}H_{12}NS]$ 238.0690, Found 238.0688.

Preparation of 1e:

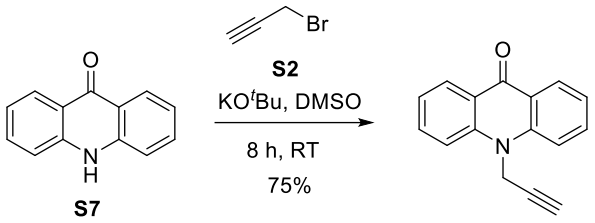

A suspension of acridone **S7** (500 mg, 2.56 mmol) and KO^{t}Bu (431 mg, 3.84 mmol) in DMSO was stirred at room temperature for 30 min. Then, it was added to a solution of propargyl bromide **S2** (80% solution in toluene, 0.34 mL, 3.59 mmol) in DMSO dropwise and the reaction mixture was stirred at room temperature for 3 h. After that, it was poured into crushed ice and the aqueous solution was extracted with DCM, washed with brine and dried over Na_2SO_4. The solvent was evaporated under vacuum. The product was purified by column chromatography on silica gel (EtOAc/Hexane, 1:5) as a white solid (450 mg, 75%). **^{1}H NMR** (400 MHz, DMSO-d_6) δ 8.38 – 8.33 (m, 2H), 7.89 – 7.83 (m, 4H), 7.40 – 7.35 (m, 2H), 5.36 (d, *J* = 2.5 Hz, 2H), 3.42 (t, *J* = 2.4 Hz, 1H). **^{13}C{^{1}H} NMR** (101 MHz, DMSO-d_6) δ 176.6, 141.2, 134.3, 126.7, 121.8, 115.9, 78.7, 75.7, 35.8. HRMS (ESI) $[M+H]^+$ *m/z*: calculated for $[C_{16}H_{12}NO]$ 234.0919, Found 234.0915.

Preparation of 2a-j: All azide derivatives were synthesized following previously reported procedures.[1-8]

4.0 Synthesis of 1,4- and 1,5-triazoles: BPTC was synthesized from alkyne **1b** (1 equiv) and azide **2d** (2.5 equiv) in presence of $CuSO_4{\cdot}5H_2O$ (0.1 equiv) and sodium ascorbate (0.2 equiv) in ^{t}BuOH and H_2O at room temperature for 12 h. **BPTC-S** was synthesized using alkyne **1b** (1 equiv) and azide **2d** (2.5 equiv) in the presence of $Cp^*RuCl(PPh_3)_2$ (0.05 equiv) in dry toluene at 80 °C for 36 h.

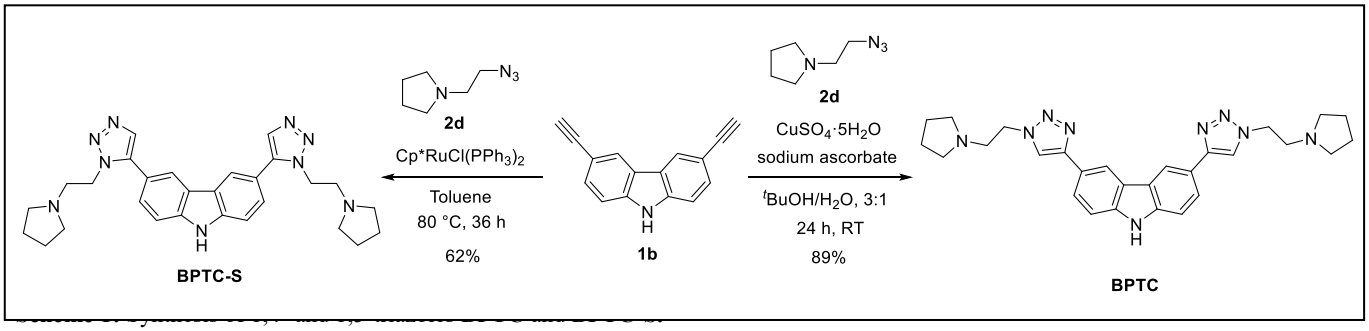

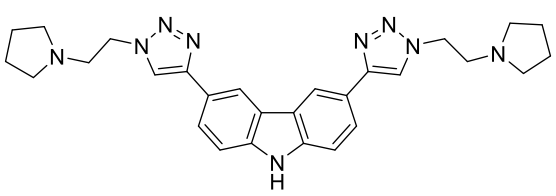

BPTC

4.1 Synthesis of BPTC: Alkyne **1b** (100 mg, 0.46 mmol) was dissolved in ^{t}BuOH and H_2O (5 mL, ^{t}BuOH/H_2O, 3:1). To this solution, $CuSO_4{\cdot}5H_2O$ (11.6 mg, 0.05 mmol) and sodium ascorbate (18.4 mg, 0.09 mmol) were added. Subsequently, azide **2d** (156 mg, 1.12 mmol) was added, and the reaction mixture was stirred at room temperature for 24 h. Upon completion, the reaction mixture was concentrated, and the crude product was purified by column chromatography on silica gel using MeOH/ammonical CH_2Cl_2 (2:98) as the eluent, affording the desired triazole product as a white solid (205 mg, 89% yield). ^{1}H NMR (500 MHz, Methanol-d_4) δ 8.56 (d, *J* = 1.6 Hz, 2H), 8.34 (s, 2H), 7.87 (dd, *J* = 8.5, 1.6 Hz, 2H), 7.52 (d, *J* = 8.4 Hz, 2H), 4.61 (t, *J* = 6.6 Hz, 4H), 3.09 (t, *J* = 6.6 Hz, 4H), 2.64 (t, *J* = 5.9 Hz, 8H), 1.84 – 1.78 (m, 8H). **^{13}C{^{1}H} NMR** (126 MHz, Methanol-d_4) δ 150.1, 142.0, 125.1, 124.7, 122.8, 121.8, 118.6, 112.4, 56.5, 55.1, 50.2, 24.3. HRMS (ESI) $[M+H]^+$ *m/z*: calculated for $[C_{28}H_{34}N_9]$ 496.2937, Found 496.2936.

4.2 Synthesis of BPTC-S: Alkyne **1b** (200 mg, 0.93 mmol) was dissolved anhydrous toluene (10 mL). To this solution, Cp*RuCl(PPh_3)$_2$ (37 mg, 0.05 mmol) was added. Subsequently, azide **2d** (130 mg, 0.93 mmol) was added, and the reaction mixture was stirred at 80 °C for 36 h. Upon completion, the reaction mixture was concentrated, and the crude product was purified by column chromatography on silica gel using MeOH/ammonical CH_2Cl_2 (5:95) as the eluent, affording the desired triazole product as a pale-yellow solid (286 mg, 62% yield). **^{1}H NMR** (500 MHz, Methanol-d_4) δ 8.30 (d, J = 1.6 Hz, 2H), 7.78 (s, 2H), 7.65 (d, J = 8.3 Hz, 2H), 7.54 (dd, J = 8.4, 1.7 Hz, 2H), 4.61 (t, J = 6.9 Hz, 4H), 2.87 (t, J = 6.9 Hz, 4H), 2.35 (t, J = 5.3 Hz, 8H), 1.67 – 1.60 (m, 8H). **^{13}C{^{1}H} NMR** (126 MHz, Methanol-d_4) δ 142.4, 140.9, 133.7, 128.1, 124.4, 122.5, 118.7, 112.9, 56.2, 54.9, 49.5, 24.2. HRMS (ESI) $[M+H]^+$ *m/z*: calculated for $[C_{28}H_{34}N_9]$ 496.2937, Found 496.2934.

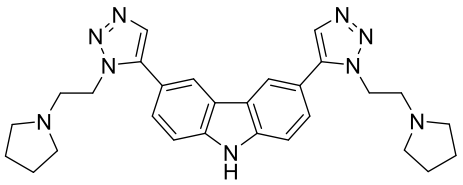

5.0 General procedure for DNA•Au@Fe_3O_4 templated cycloaddition

To a suspension of DNA nanotemplate (10 µL), alkynes **1a-e** (individually) and azides **2a-j** were added, and the volume was adjusted to 50 µL using the corresponding buffer. For G_4 DNA and *ds*DNA, the buffer used was 60 mM sodium cacodylate buffer, pH 7.2 and for i-motif (iM) DNA, the buffer was 10 mM sodium cacodylate buffer, pH 5.5). The final concentrations of the components were as follows: alkyne (1 µM) and azide (4 µM), DNA at approximately 4-5 µM.

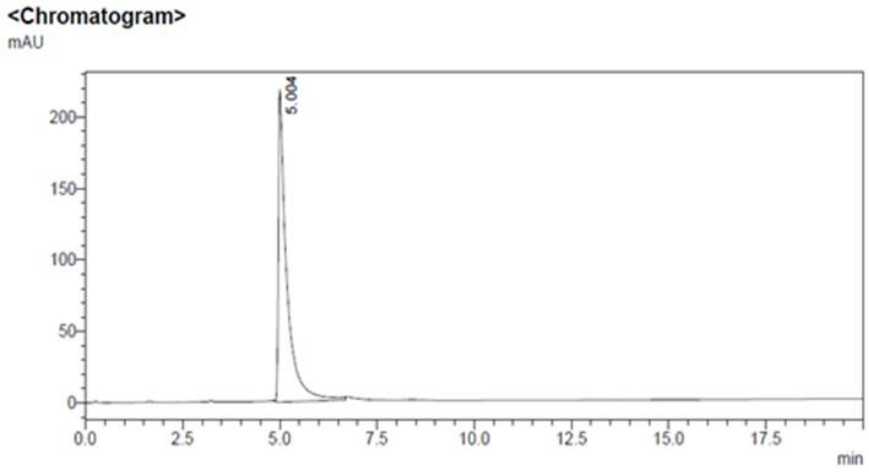

<Peak Table>

Peak#	Ret. Time	Area	Height	Area%	Height%
1	5.004	3216145	219063	100.000	100.000
Total		3216145	219063	100.000	100.000

Fig. S1. HPLC trace of the hit triazole product **BPTC**.

The reaction mixture, containing the DNA nano-template and azide-alkyne building blocks, was continuously shaken at room temperature for 4 days. After 4 days of incubation, the DNA nanotemplates were separated from the reaction mixture using magnet decantation and washed thrice with the respective buffer to remove the unreacted starting materials. Subsequently, the nanotemplates were dispersed in 50 µL of the corresponding buffer,and the dispersion was heated at 65 °C for 5 min in the presence of 1 M LiCl. The nanotemplates were instantly separated by magnetic decantation, and the supernatant was analysed by HPLC. The HPLC fractions corresponding to different peaks were identified by ESI-MS spectrometry. The HPLC analysis was performed using 5.0 µm ODS2 reverse phase column (4.6×250 mm) at 290 nm detection wavelength. Flow rate was 0.5 ml min^{-1} CH_3CN/H_2O (90:10) containing 0.1% TFA over 20 min.

6.0 Monitoring DNA•Au@Fe_3O_4-mediated *in-situ* click reaction by HPLC analysis

The DNA nanotemplated reactions were performed in presence of various thiolated DNA as well as only Au-coated Fe nanotemplate.

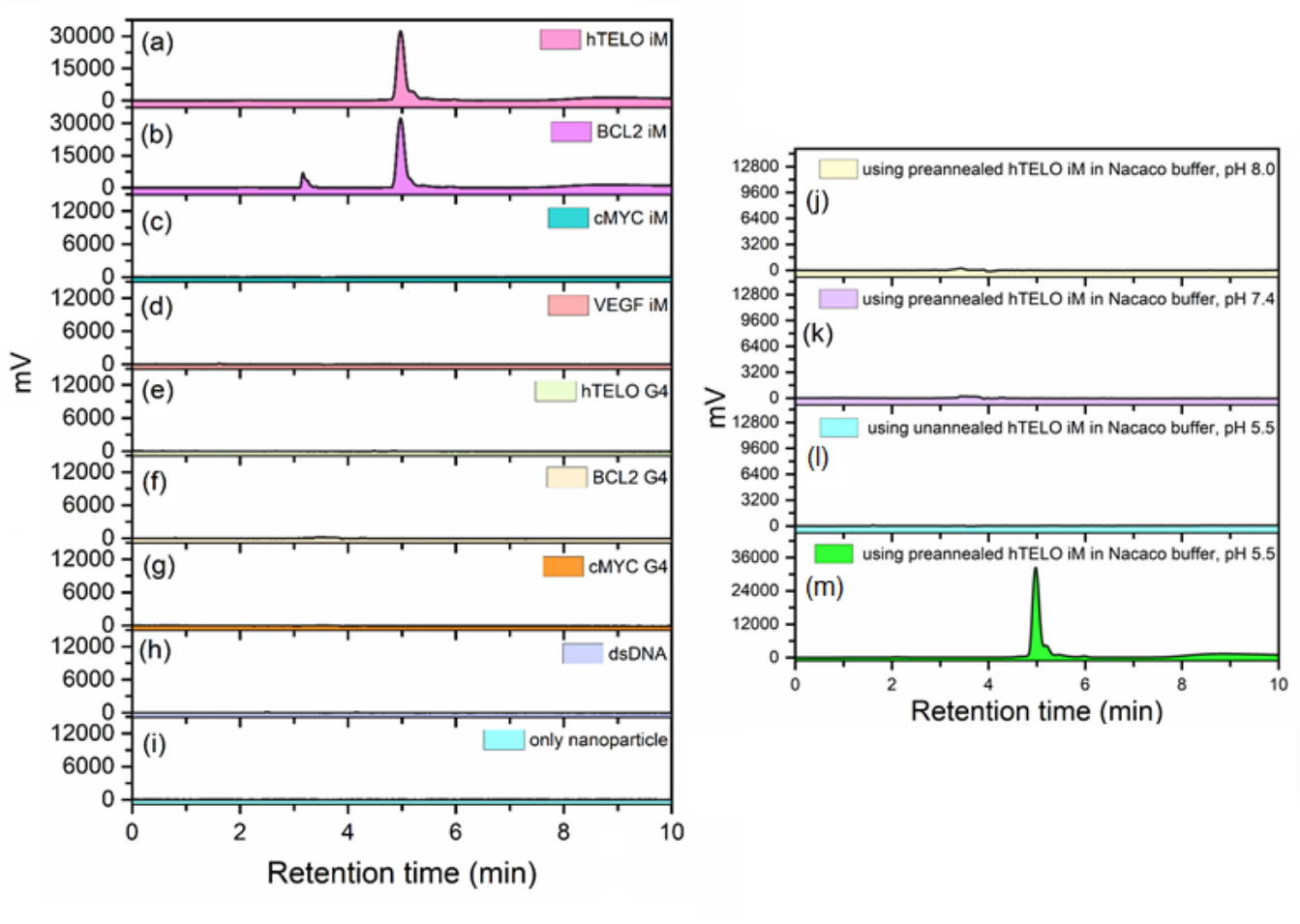

Fig. S2. HPLC chromatograms of the reaction mixture obtained using (a) *h-TELO* iM•Au@Fe_3O_4, (b) *BCL2* iM•Au@Fe_3O_4, (c) *c-MYC* iM•Au@Fe_3O_4, (d) *VEGF* iM•Au@Fe_3O_4 respectively in 10 mM Na-cacodylate buffer (pH 5.5), (e) *h-TELO* G4•Au@Fe_3O_4, (f) *BCL2* G4•Au@Fe_3O_4, (g) *c-MYC* G4•Au@Fe_3O_4, (h) *ds*DNA•Au@Fe_3O_4 respectively in 60 mM Na-cacodylate buffer (pH 7.2),, (i) Au@Fe_3O_4 nanotemplates in 10 mM Na-cacodylate buffer (pH 5.5), and (j) preannealed *h-TELO* iM•Au@Fe_3O_4 in 10 mM Na-cacodylate buffer (pH 8.0), (k) preannealed *h-TELO* iM•Au@Fe_3O_4 in 10 mM Na-cacodylate buffer (pH 7.4), (l) unannealed *h-TELO* iM•Au@Fe_3O_4 in 10 mM Na-cacodylate buffer (pH 5.5) and (m) preannealed *h-TELO* iM•Au@Fe_3O_4 in 10 mM Na-cacodylate buffer (pH 5.5) synthesized from alkyne **1b** and azide **2d.**

7.0 Determination of the regiochemistry of the lead triazole product (BPTC)

The regiochemistry of the lead triazole compound (**BPTC**), generated by DNA•Au@Fe_3O_4 was determined by comparing the HPLC traces of the templated cycloaddition (*in-situ* reaction) with the typical thermal, Cu-(I) catalyzed reactions as well as Ru-catalyzed reactions between the corresponding alkyne and azide fragments.

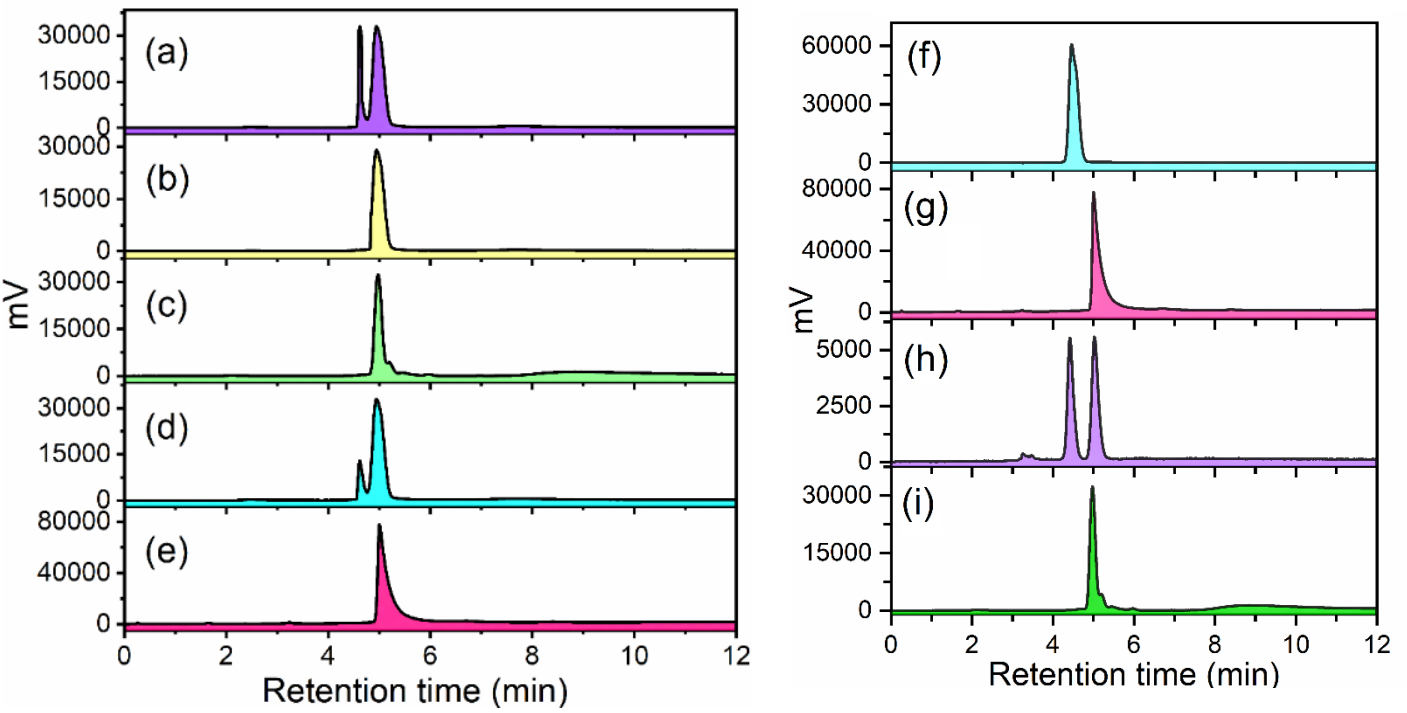

Fig. S3. HPLC traces of the products obtained in the 1, 3-dipolar cycloaddition between alkyne **1b** and azide **2d** obtained under different conditions; (a) products when the reaction carried out at 70 °C for 24 h, (b) product of *in-situ* reaction carried out using *BCL2* iM•Au@Fe_3O_4 DNA nanotemplate, (c) product of *in-situ* reaction carried out using *h-TELO* iM•Au@Fe_3O_4 DNA nanotemplate, (d) co-injection of *in-situ* cycloaddition product and thermal products, (e) Cu-(I) catalyzed cycloaddition reaction product, (f) pure 1,5-triazole product obtained via Ru catalyzed cycloaddition reaction, (g) pure 1,4-triazole product obtained via Cu catalyzed cycloaddition reaction, (h) co-injection of 1,4- and 1,5-triazole product, (i) product of *in-situ* reaction carried out using *h-TELO* iM•Au@Fe_3O_4 DNA nanotemplate.

8.0 ^{1}H and $^{13}C\{^{1}H\}$ NMR spectra of compounds

8.1 ^{1}H and $^{13}C\{^{1}H\}$ NMR spectra of 1a:

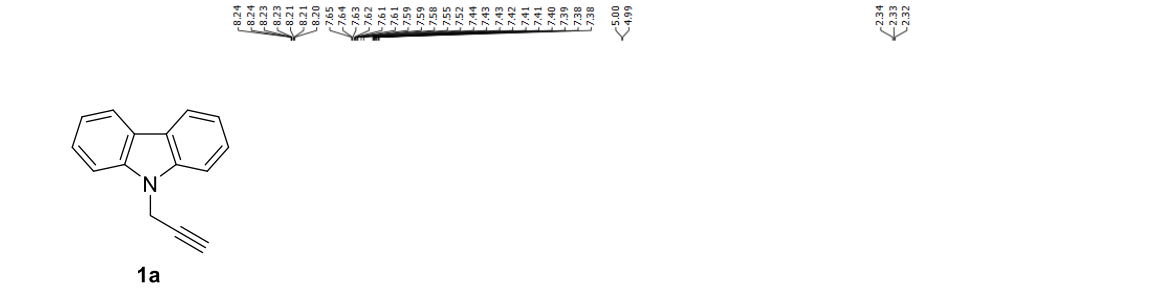

1a

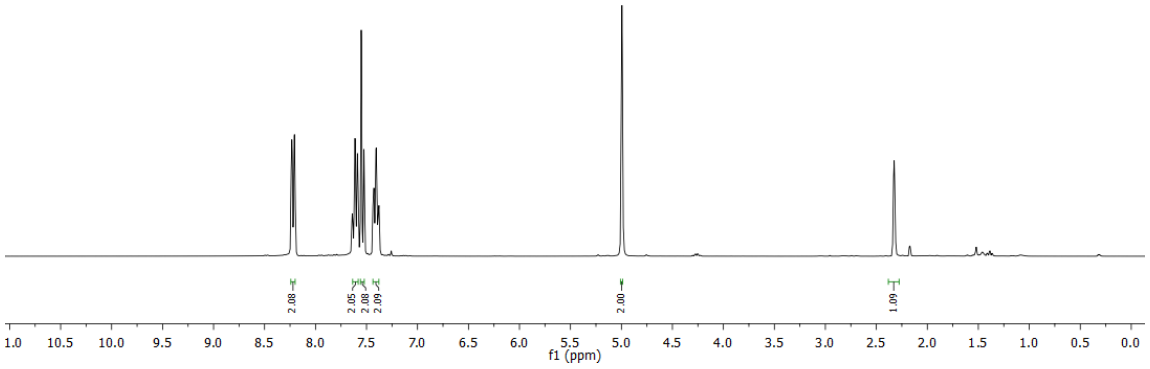

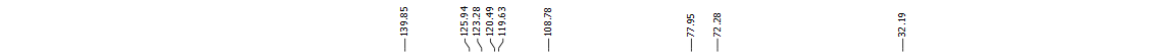

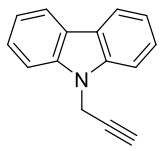

1a

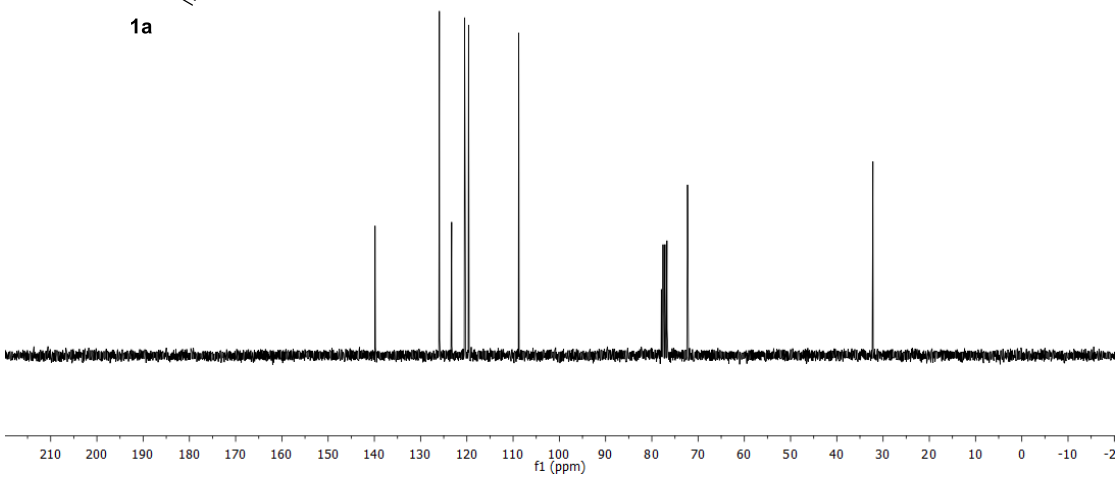

8.2 ^{1}H and $^{13}C\{^{1}H\}$ NMR spectra of 1b:

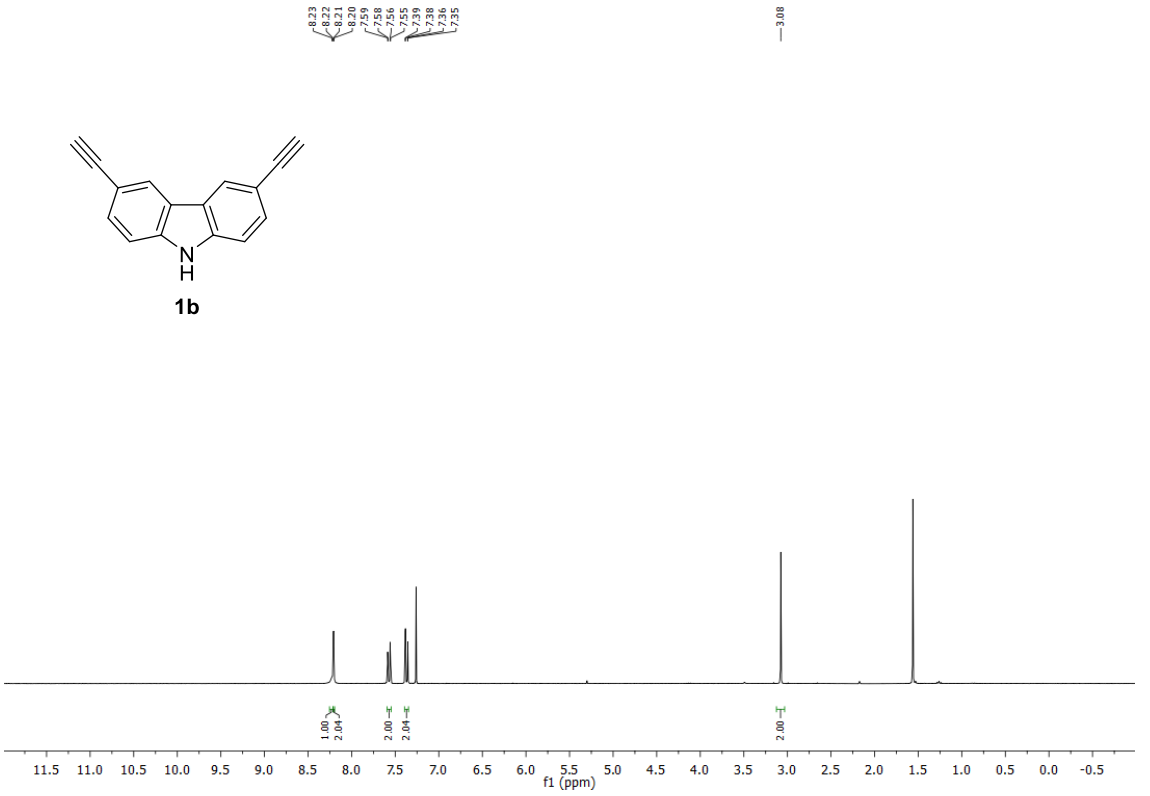

1b

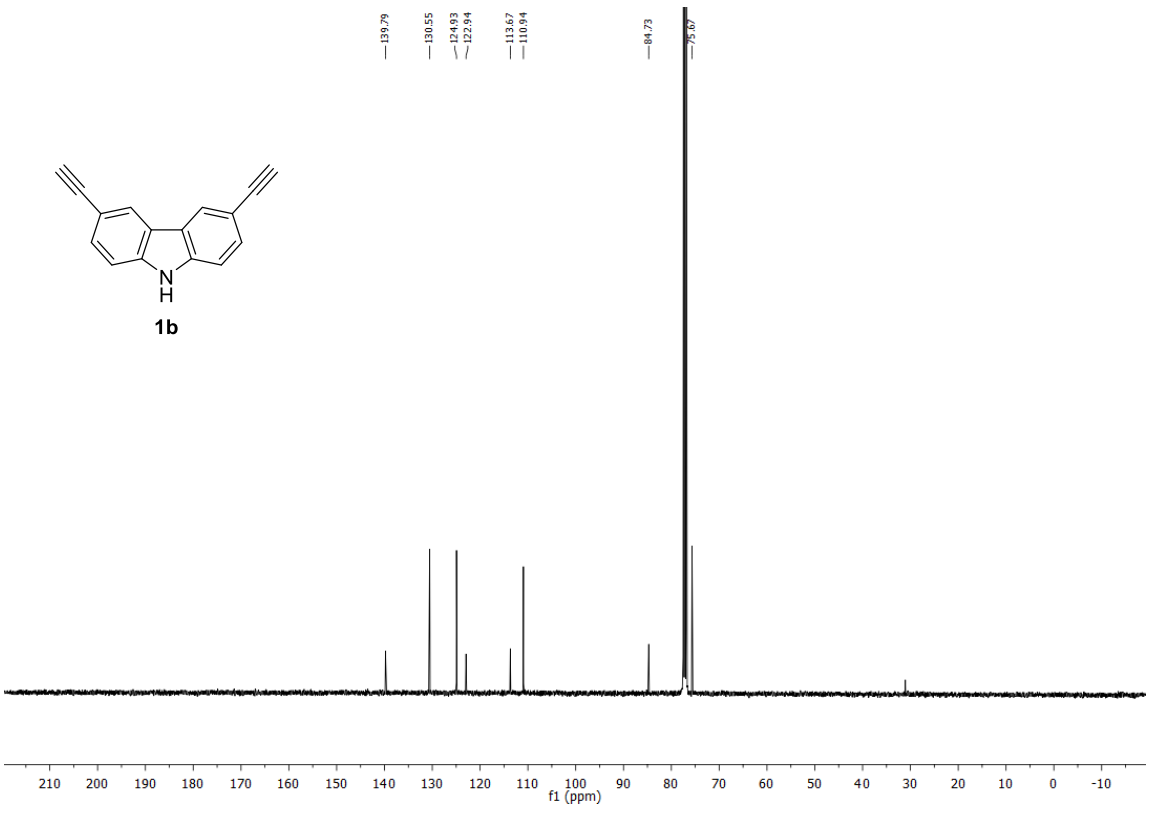

1b

8.3 ^{1}H and $^{13}C\{^{1}H\}$ NMR spectra of 1c:

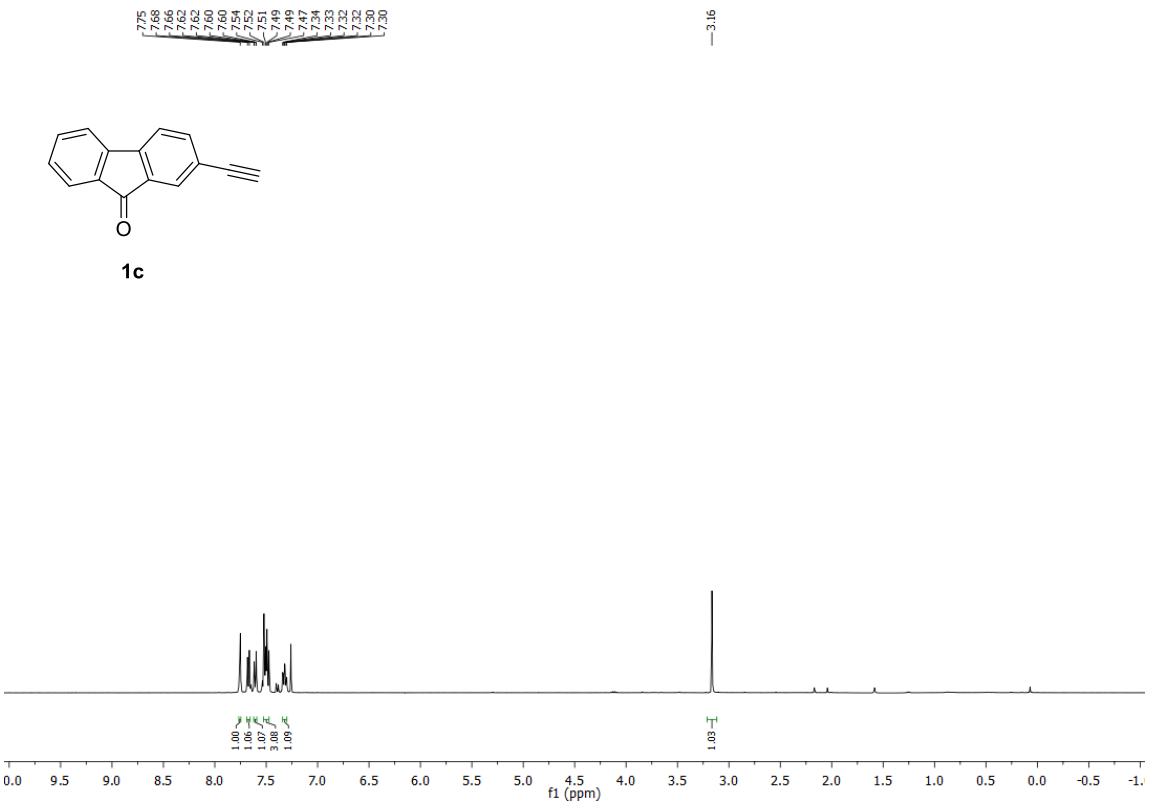

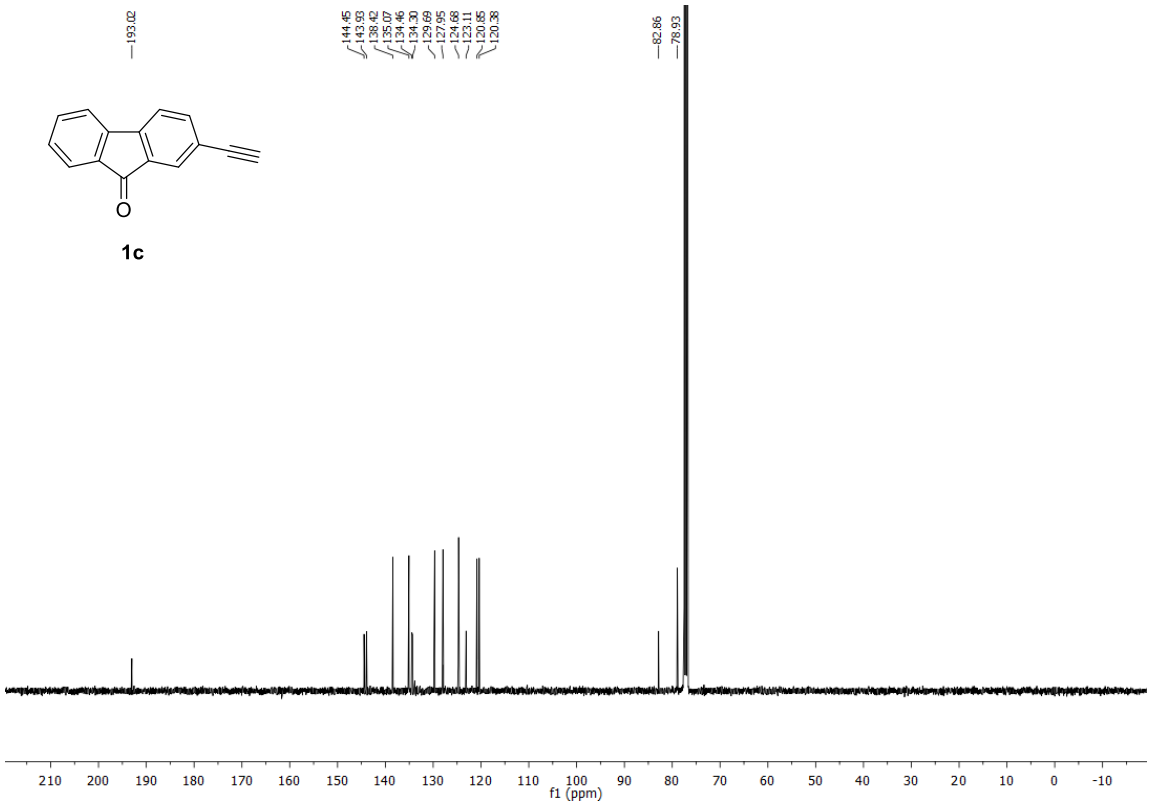

8.4 ^{1}H and $^{13}C\{^{1}H\}$ NMR spectra of 1d:

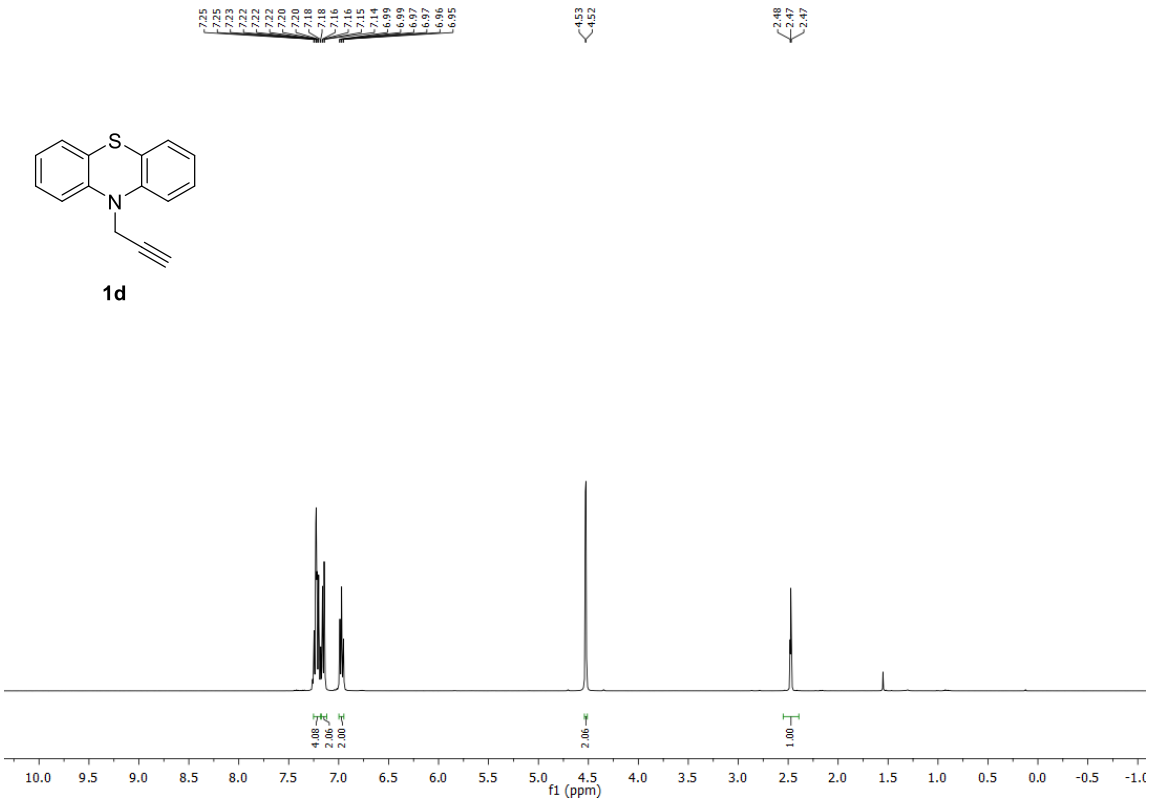

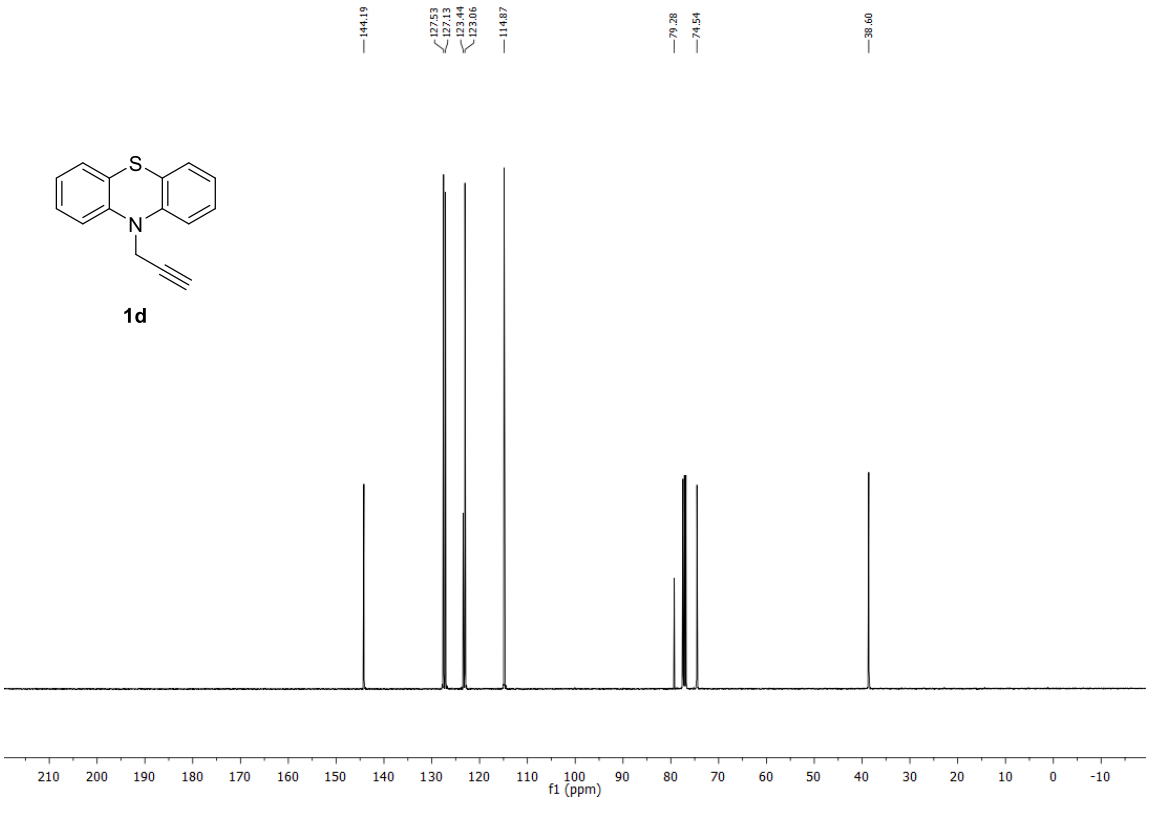

8.5 ^{1}H and $^{13}C\{^{1}H\}$ NMR spectra of 1e:

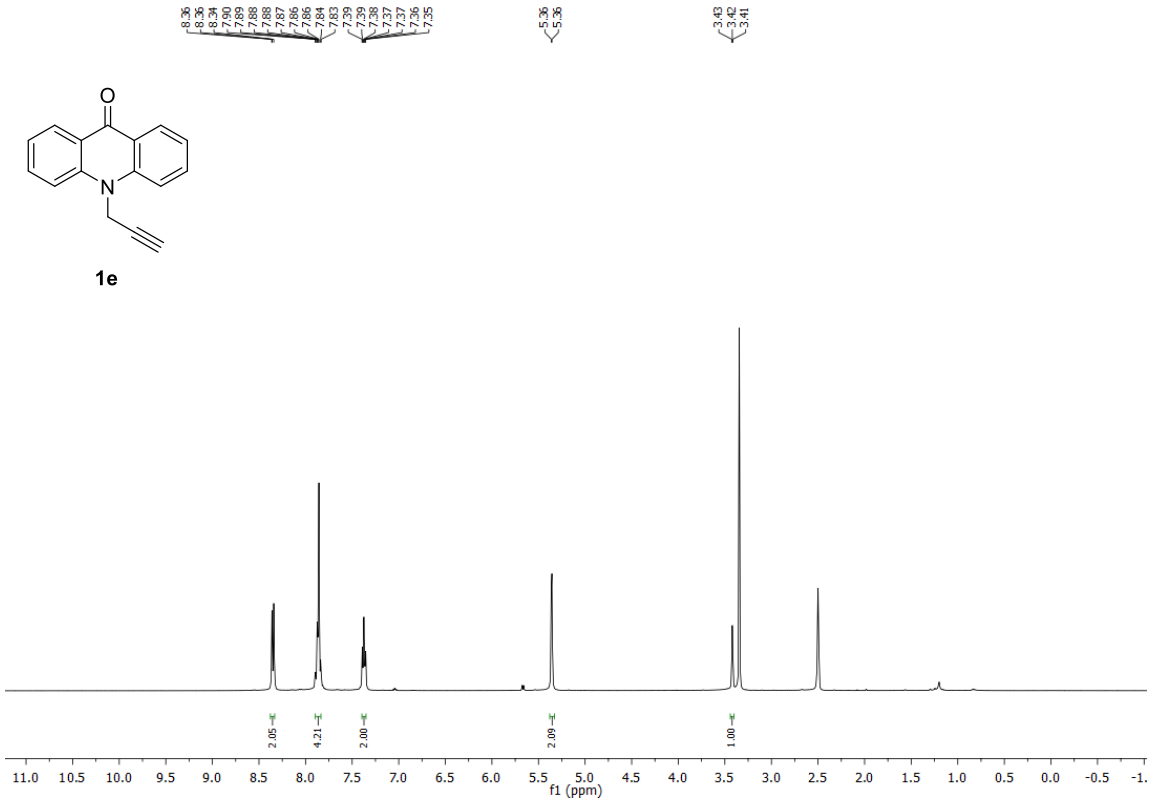

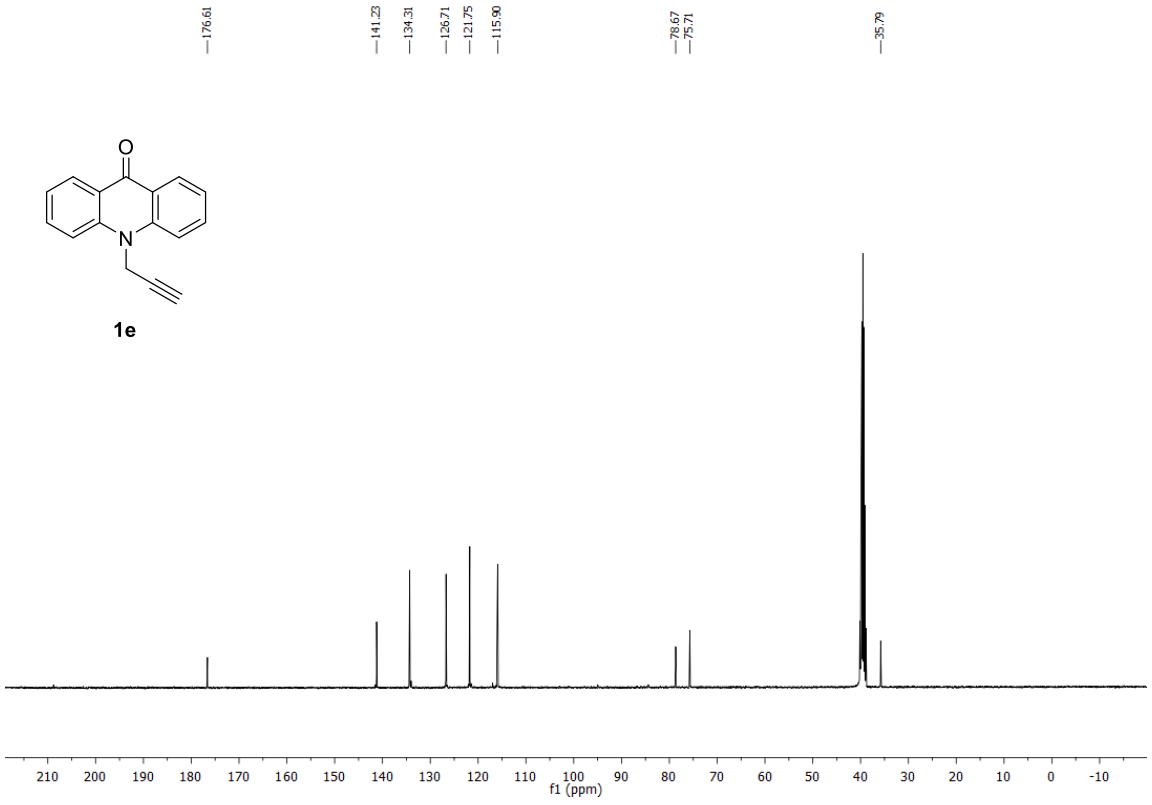

8.6 ^{1}H and $^{13}C\{^{1}H\}$ NMR spectra of BPTC:

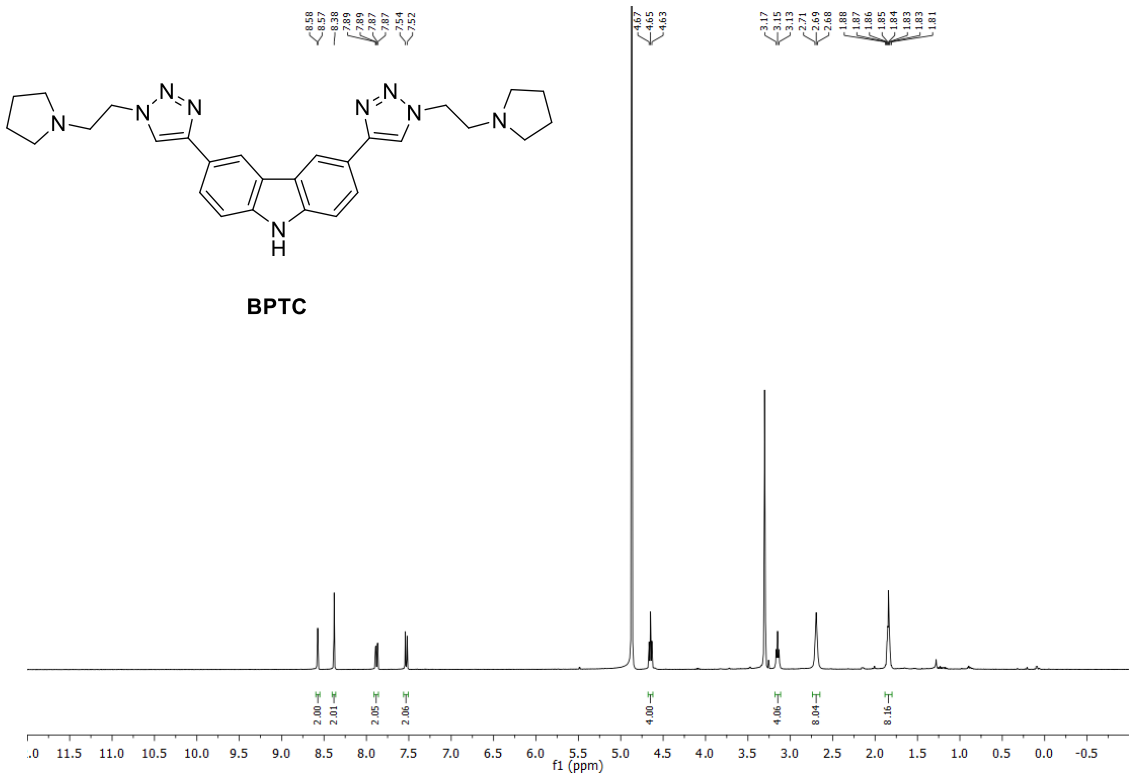

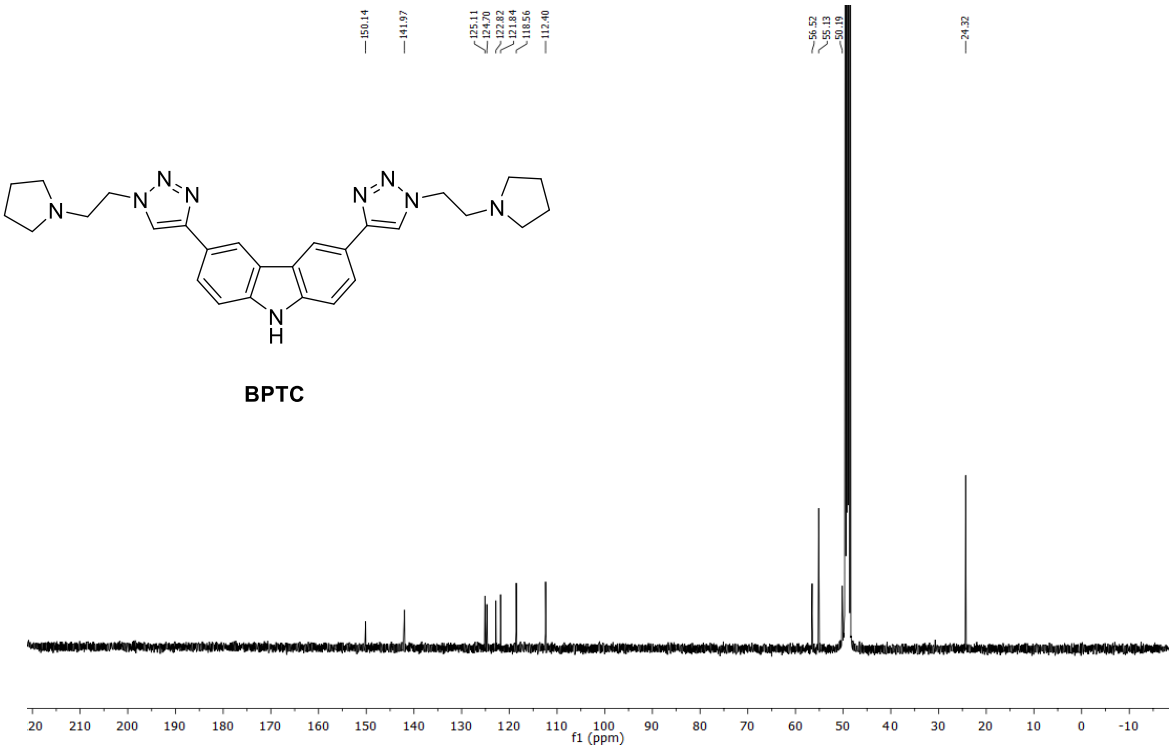

8.7 ^{1}H and $^{13}C\{^{1}H\}$ NMR spectra of BPTC-S:

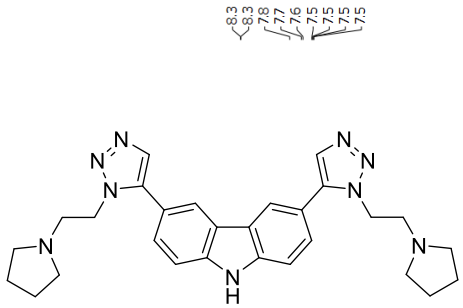

BPTC-S

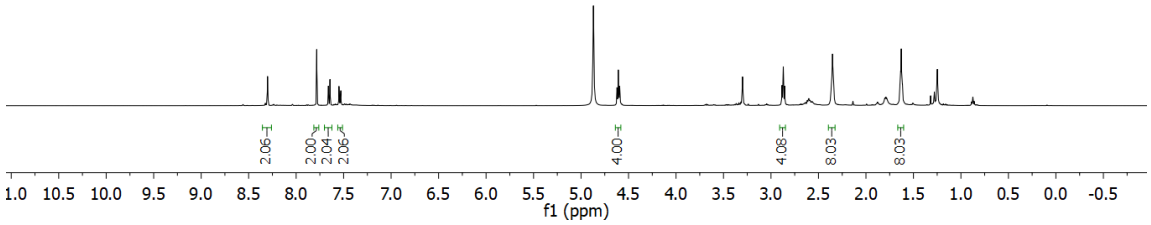

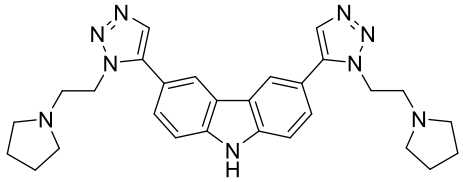

BPTC-S

9.0 FRET melting analysis

FRET melting experiments were performed using 0.2 μM concentration of 5'- FAM and 3'-TAMRA labelled DNA sequences. FRET melting experiments with G-quadruplex DNA and duplex DNA were carried out in 60 mM sodium cacodylate buffer (pH 7.2) and the FRET melting assay with i-motif DNA sequences were carried out in 10 mM sodium cacodylate buffer (pH 5.5). The DNA sequences were annealed by heating at 95 °C for 5 min followed by gradual cooling to room temperature at a controlled rate of 0.1 °C min^{-1} and then kept at 4 °C for overnight. The assay was carried out on a real-time PCR apparatus (Light Cycler 480 II System) by incubating the dual labelled DNA oligonucleotides (0.2 μM) with each 0.5, 1.0 and 1.5 μM of the lead triazole derivative (**BPTC**) separately for 1 h. To perform competition experiments, dual labeled C-rich sequences (*h-TELO* and *BCL2* iM) were annealed in 10 mM sodium cacodylate buffer (pH 5.5) as described before to form i-motifs. In dual labeled i-motifs, 50 equivalent excess of annealed competitor *c-MYC* iM and duplex DNA were added. The concentration of **BPTC** was kept at 1.5 μM. Fluorescence measurements were taken with an excitation wavelength of 483 nm and a detection wavelength of 533 nm at intervals of 1°C over the range of 37–95°C. Melting temperatures were calculated using Origin Pro 8 data software. Dual fluorescently labelled DNA oligonucleotides used in these experiments are:

c-MYC iM (T_m ~ 56.2 °C): 5'-FAM-TCCCCACCTTCCCCACCCTCCCCACCCTCCCCA-TAMRA-3'

BCL2 iM (T_m ~ 54.0 °C): 5'-FAM-CAGCCCCGCTCCCGCCCCCTTCCTCCCGCGCCCGCCCCT-TAMRA-3'

h-TELO iM (T_m ~ 44.0 °C): 5'-FAM- TTCTTGAATCCCAATCCCAATCCCAATCCCAA-TAMRA-3'

c-MYC G4 (T_m ~ 68.3 °C): 5'-FAM-TGGGGAGGGTGGGGAGGGTGGGGAAGG-TAMRA-3'

BCL2 G4 (T_m ~ 52.1 °C): 5'-FAM-AGGGGCGGGCGCGGGAGGAAGGGGGCGGGAGCGGGGCTG-TAMRA-3'

h-TELO G4 (T_m ~ 41.2 °C): 5'-FAM- TTGGGTTAGGGTTAGGGTTAGGGA-TAMRA-3'

*ds*DNA (T_m ~ 73.4 °C): 5'-FAM-CAAAAATTTTTGCAAAAATTTTTG-TAMRA-3

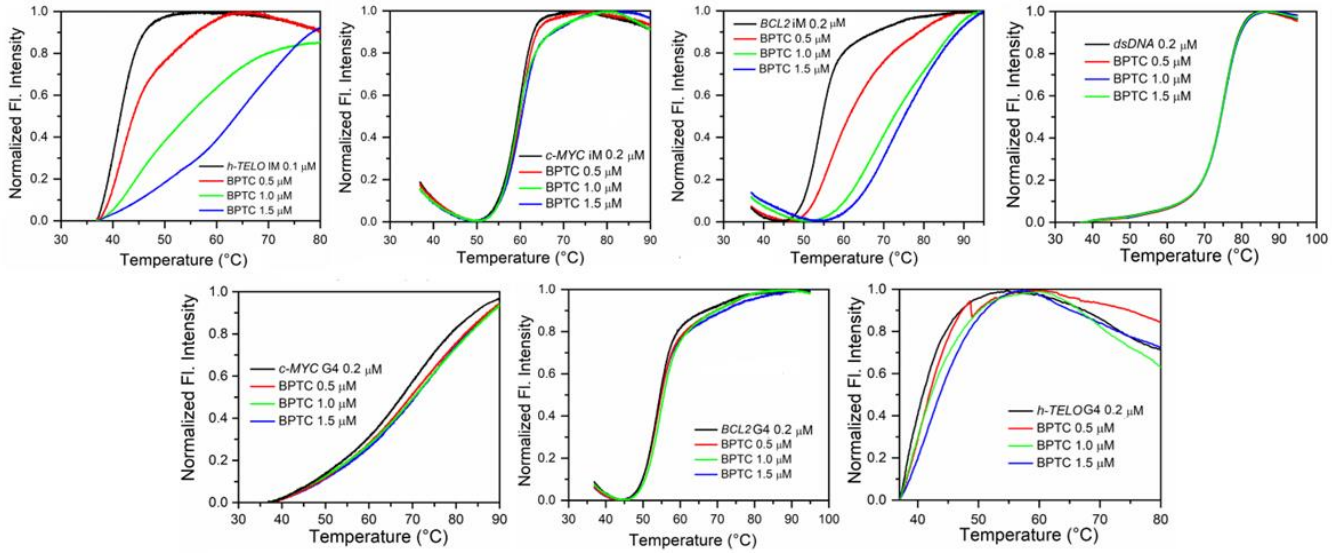

Fig. S4. FRET melting curves of 0.2 μM 5'-FAM and 3'-TAMRA labelled DNA sequences with incremental addition of **BPTC** in 10 mM Na-cacodylate buffer (pH 5.5) for i-motif DNAs and in 60 mM Na-cacodylate buffer (pH 7.2) for G-quadruplex DNAs as well as *ds*DNA respectively as indicated in the figures.

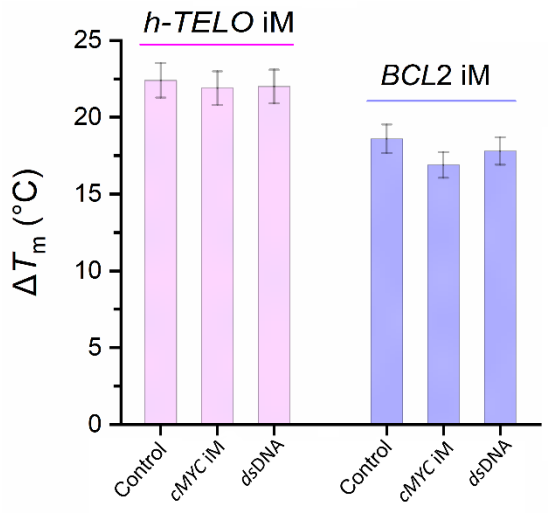

Fig. S5. FRET competition of **BPTC** bound dual labeled *h-TELO* and *BCL2* i-motifs in presence of 50 equivalent of competitor *c-MYC* iM and duplex DNA (10 mM Na-cacodylate buffer, pH 5.5).

10.0 Fluorimetric spectroscopic titration

The fluorescence spectra were recorded on a Horiba Jobin Yvon Fluoromax-3 spectrofluorometer at 25 °C using a 10 mm path-length quartz cuvette and filtered buffer solutions. For G-quadruplex and duplex DNA, a 60 mM sodium cacodylate buffer (pH 7.2) was used, while for i-motif DNA, a 10 mM sodium cacodylate buffer (pH 5.5) was employed. Fluorescence titrations were performed by successive addition of DNA solution (0.0–2.0 μM) into a 2 μM ligand solution, and the fluorescence response was monitored accordingly. The emission was measured from the wavelength range of 355 – 500 nm (λ_{ex} = 338 nm). The data were plotted with Origin 8.0 software and fitted with the equation given below.

$$F = F_0 + \frac{(F_{max} - F_0)\,[DNA]}{k_d + [DNA]} \quad \text{.....Equation 1.}$$

Where, F is the fluorescence intensity, F_{max} is the maximum fluorescence intensity, and F_0 is the fluorescence intensity in the absence of DNA and K_d indicates the dissociation constant.

c-MYC iM: 5’-TCCCCACCTTCCCCACCCTCCCCACCCTCCCCA-3’

BCL2 iM: 5’-CAGCCCCGCTCCCGCCCCCTTCCTCCCGCGCCCGCCCCT-3’

h-TELO iM: 5’-AACCCTAACCCTAACCCTAACCCTAAGTTCTT-3’

c-MYC G4: 5’-TGGGGAGGGTGGGGAGGGTGGGGAAGG-3’

BCL2 G4: 5’-AGGGGCGGGCGCGGGAGGAAGGGGGCGGGAGCGGGGCTG-3’

h-TELO G4: 5’- TTGGGTTAGGGTTAGGGTTAGGGA-3’

*ds*DNA: 5’-CAAAAATTTTTGCAAAAATTTTTG-3’

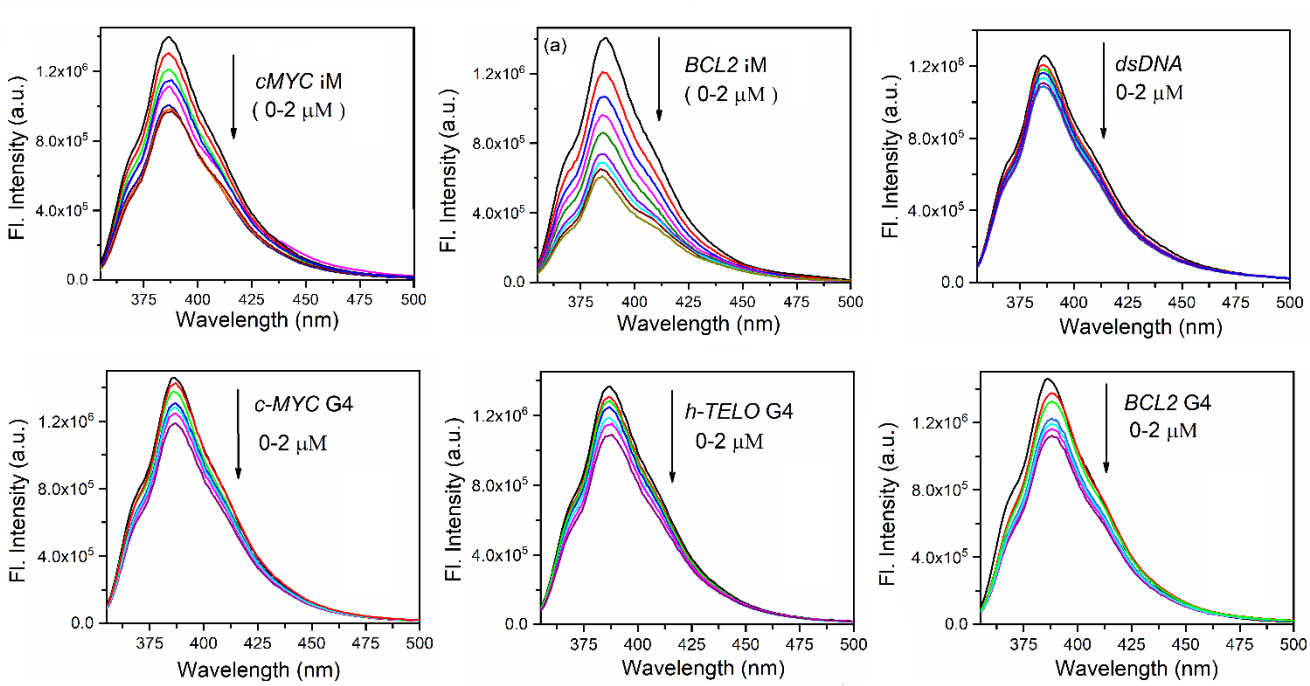

Fig. S6. Fluorescence titrations of 2 μM **BPTC** with incremental addition of i-motif DNAs in 10 mM Na-cacodylate buffer (pH 5.5) and with G-quadruplex DNAs as well as *ds*DNA respectively in 60 mM Na-cacodylate buffer (pH 7.2) as indicated in the figures.

11.0 Circular dichroism spectroscopy

Circular dichroism (CD) spectra were acquired on a Jasco J815 model unit (Jasco International Co. Ltd.) equipped with a Jasco temperature controller (PFD 425L/15) at 298.15 ± 0.5 *K* following the protocols described in details previously. A rectangular strain free quartz cuvette of 1 mm path length was used. Titrations were performed by the addition of increasing concentrations of **BPTC** to a fixed concentration (10 μM) of iM DNAs, G4 DNAs and *ds*DNA. The molar ellipticity values [θ] were calculated from the equation $[\theta]=100\times\theta/(C\times l)$, where θ is the observed ellipticity in milli degrees, C is the concentration in moles/lit, and l is the cell path length of the cuvette in cm. The molar ellipticity $[\theta]$ (deg.cm^2/dmol) values are expressed in terms of base pairs in the region 200–400 nm. The CD spectra represented an average of three scans, correction for dilution effects was performed in each.

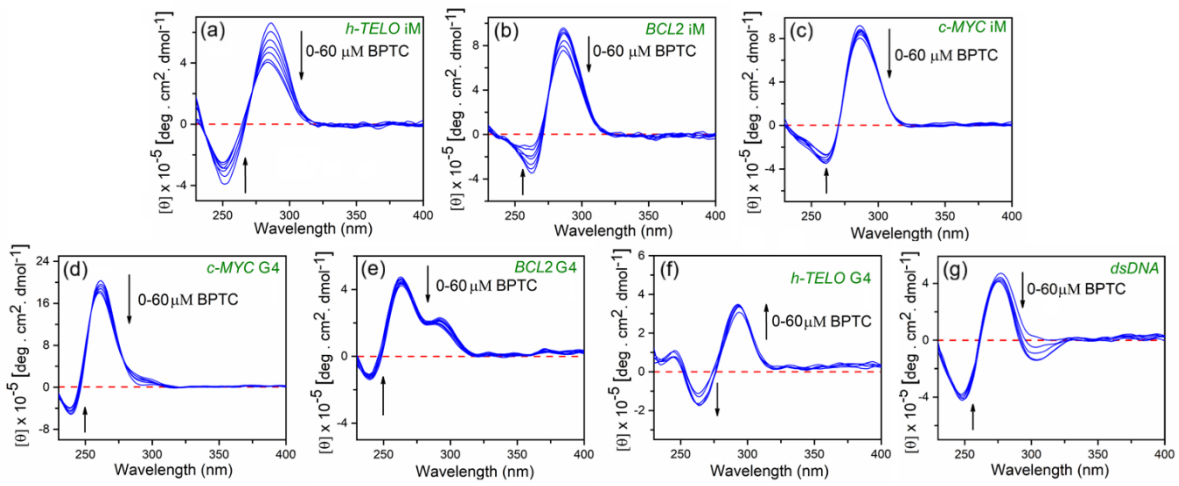

Fig. S7. CD spectra of (a) *h-TELO* iM DNA (10 μM), (b) *BCL2* iM DNA (10 μM), (c) *c-MYC* iM DNA (10 μM) in 10 mM Na-cacodylate buffer (pH 5.5) upon addition of the incremental amount of **BPTC** (0-60 μM); (d) *c-MYC* G4 DNA (10 μM), (e) *BCL2* G4 DNA (10 μM), (f) *h-TELO* G4 DNA (10 μM) and (g) *ds*DNA (10 μM) in 60 mM Na-cacodylate buffer (pH 7.2). Each CD spectrum represented as an average of three scans, correction for dilution effects was performed in each case.

12.0 Isothermal titration calorimetry (ITC) studies

Isothermal titration calorimetry experiments were performed on a VP-ITC microcalorimeter (Malvern Instruments, United Kingdom) to study the binding interaction of **BPTC** with iM DNA. The data were analysed using Origin 7.0 software to obtain the thermodynamic parameters by following the protocols described in details previously. Buffer solutions were degassed extensively to prevent air bubble formation during titration. Titrations were performed by injecting **BPTC** solution (400 μM) from the rotating syringe into the isothermal chamber containing 1.4235 mL of DNA solutions (20 μM) at 298.15 K. The titration was performed in 28 sequential injections and each injection released 10 μL aliquots from the rotating syringe into the calorimeter cell. The corresponding dilution study of each reaction was performed in separate experiment by injecting identical volumes of the same concentration of the **BPTC** into the buffer alone. The heat associated with each injection was observed as a heat spike which is actually the measure of the power needed to maintain the sample and reference cells at same temperatures. The area under each peak was integrated to obtain the heat associated with that injection. The heats of dilution were subtracted from the corresponding heat associated with the binding experiment that afforded the actual heat of **BPTC**-iM DNA interaction. The corrected injection heats were thereafter plotted as a function of the molar ratio and this was fitted with a model for one set of binding sites to calculate the equilibrium constant (K), the binding stoichiometry (N) and the standard molar enthalpy change (ΔH^0) of association. The standard molar Gibbs energy change (ΔG^0) was calculated using the standard relationship

$$\Delta G^0 = -RT \ln K \qquad (2)$$

Where, R (1.987 cal K^{-1} mol^{-1}) is the gas constant and T is the temperature in kelvins (K). Analysis of ITC data (Table S1) yielded the values of standard molar Gibbs energy and standard molar enthalpy change that enabled the calculation of $T\Delta S^0$, where ΔS^0 is the calculated standard molar entropy change, using the relationship

$$T\Delta S^0 = \Delta H^0 - \Delta G^0 \qquad (3)$$

The reciprocal of equilibrium constant (K) was used to evaluate the corresponding K_d values.

Table S1. Thermodynamic Factors for the Association of **BPTC** with *h-TELO* and *BCL2* iM DNA at 298.15 K

	$K \times 10^6$ M^{-1}	K_d (μM)	ΔH^o (kcal mol^{-1})	$T\Delta S^o$ (kcal mol^{-1})	ΔG^o (kcal mol^{-1})	N
h-TELO iM-**BPTC**	1.26±0.01	0.79±0.01	-1.345±0.01	6.976±0.01	-8.321±0.01	0.83±0.01
BCL2 iM-**BPTC**	0.78±0.12	1.27±0.12	-1.990±0.01	6.052±0.01	-8.042±0.01	0.94±0.01

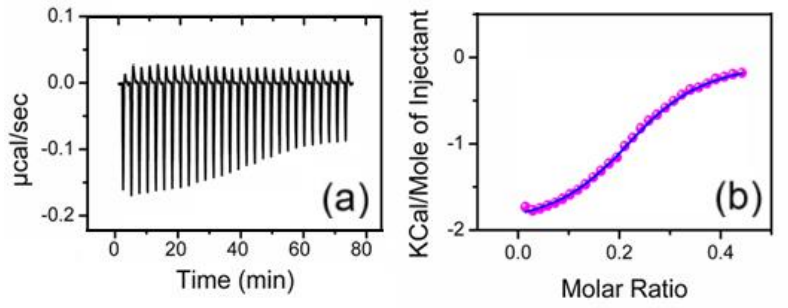

Fig. S8. The raw data resulting from the sequential injection of **BPTC** into *BCL2* iM DNA solution. The corresponding normalized heat signals versus molar ratio. The data points (•) show the experimental injection heats, while the continuous lines show the best-fit curve to the experimental data. The concentration of the iM DNA in the calorimeter cell was 20 μM and aliquots of **BPTC** (400 μM) were titrated. ITC data were recorded at T = 298.15 K.

Table S2. Comparison of **BPTC** with existing iM ligands from iM-LDB.

Ligand	**Gene/ DNA sequence**	**Effect on iM**	**K_d value (μM)**	**References**
Mitoxantrone	Telomere	Destabilization	K_d = 12 ± 3 μM (SPR)	9
	c-MYC	Stabilization	K_d = 12 ± 3 μM (SPR)	
Berberine	Telomere	Low binding	K_d = 19.6 μM (pH 6.01) (fluorescence titration)	10
Tobramycin	Telomere	-	K_d = 17±2.0 (pH 5.5) (SPR)	11
PBP1	*BCL2*	Stabilization	K_d = 0.3 μM (Fluorescence Titration)	12
	c-MYC	Stabilization	K_d = 2.4 μM (Fluorescence Titration)	
3be	*c-MYC*	Stabilization	K_d = 0.25 μM (Fluorescence Titration)	13
3bm	*BCL2*	Low binding	K_d = 1.18 μM (Fluorescence Titration)	
A22	*BCL2*	Stabilization	K_d =3.56 μM (SPR)	14
IMC-76	*BCL2*	Destabilization	K_d = 1.01 μM (FRET Assay)	15
IMC-48	*BCL2*	Stabilization	K_d = 0.49 μM (FRET Assay)	
A9	*c-MYC*	Stabilization	K_D = 2.4 μM (SPR)	16
B19	*c-MYC*	Stabilization	K_D =7.8 μM (SPR)	17
ActD	*c-MYC*	Stabilization	$K_b = 9.3\times10^4$ M^{-1} (Fluorescence Titration)	18
Compound 1	*HRAS*	Low binding	K_D = 7.4±5.3μM (SPR)	19
Compound 2	*HRAS*	Low binding	K_D = 5.9±3.7μM (SPR)	
Fis	*VEGF*	Destabilization	$K_a = 9.8\times10^4 M^{-1}$ (Fluorescence Titration); K_d=10.2 μM	20
$[Tb_2(DL\text{-}Cys)_4(H_2O)_8]Cl_2$	Telomere	Low binding	$K_b = 4.6\times10^4$ (fluorescence titration) K_d=21.7 μM	21
$[Tb_2(DL\text{-}HVal)_4(H_2O)_8]Cl_6.2H_2O$	Telomere	Low binding	$K_b=3.3\times10^4$ (fluorescence titration); K_d=30.3 μM	
Phenanthroline derivatives	Telomere	Stabilization	K_d ≈ 0.1–0.4 μM (fluorescence titration)	22
Crystal violet	Telomere	1:1 binding	K_d ~1.4 μM (UV-visible titration)	23
Cis-ruthenium(II)polypyridine compound	Telomere	Stabilization	$K_b=(1.13\pm0.15)\times10^6 M^{-1}$ (absorption titration); K_d=0.88 μM	24
Mer-ruthenium(II)polypyridine compound	Telomere	Stabilization	$K_b=0.63\times10^6 M^{-1}$ (absorption titration); K_d=1.58 μM	
Spermidine	C6Ti-motif	Stabilization	$K_{d\,1}$=0.003±0.001mM; $K_{d\,2}$=1.0 ±0.92mM (CD)	25
Spermine	C6Ti-motif	Stabilization	K_d =0.018±0.003mM (CD)	
Putrescine	C6Ti-motif	Stabilization	K_d =5.3±1.1mM (CD)	
Coumarin 343	Telomere	Stabilization	$K_a = 6.2\times10^5$ M^{-1} (fluorescence titration); K_d=1.61 μM	26
BPTC	Telomere	Stabilization	K_d =0.54±0.32 μM	This work
	BCL2	Stabilization	K_d =1.11±0.07 μM	

13.0 Molecular docking

The three-dimensional structure of the i-motif DNA (PDB ID: 8OFC) was retrieved from the RCSB Protein Data Bank. This structure represents a monomeric i-motif domain derived from the human telomeric C-rich strand (sequence: 5'-d(C_3TAA(C/tC)CCCTA$_3$CCCTA$_3$CCCTA$_3$)-3), forming a compact quadruplex architecture stabilized by intercalated hemiprotonated C^+ base pairs. The structure is characterized by a central cavity, which presents a potential binding site for small molecules. From a drug design perspective, such confined cavities are of particular interest, as they can promote selective ligand recognition through steric complementarity and multivalent noncovalent interactions.[27,28]

For docking studies, the monomeric unit (chain A) was selected and preprocessed using the Prepare Protein protocol in MGL Tools. This included the addition of hydrogen atoms, assignment of appropriate protonation states, modeling of missing loop regions, and removal of crystallographic water molecules and heteroatoms. Proper structural preparation is essential in structure-based drug design, as inaccuracies in protonation or geometry can significantly affect docking outcomes and interaction predictions.[29-31]

Molecular docking was performed using AutoDock Vina, employing standard protocols optimized for nucleic acid–ligand interactions. Simulations were carried out using NAMD with the CHARMM36m force field parameters for nucleic acids and ions.[32] The SwissParam server was used to generate topology and parameter files for the best-docked ligand.[33] A grid box encompassing the central cavity and adjacent groove regions was defined to allow unbiased exploration of potential binding modes. The docking procedure generated 20 distinct conformations, which were ranked based on predicted binding free energy and further evaluated through visual inspection of interaction patterns and geometric complementarity. The entire system, consisting of the i-motif, ligand, Na^+, and Cl^- ions, was subjected to energy minimization for 9,000,000 steps (45 ns). Periodic boundary conditions were defined with coordinate offsets of X: –0.113, Y: –0.102, Z: –0.068. During equilibration, positional restraints were applied to both the i-motif and the ligand. The simulation temperature was maintained at 310 K, and long-range electrostatic interactions were computed using the Particle Mesh Ewald (PME) method.[34] Trajectory analysis was conducted using VMD (version 1.9.3).

The top-ranked binding pose exhibited a favorable docking score of –11.4 kcal/mol, indicating strong binding affinity. Importantly, the ligand was consistently localized within the central cavity of the i-motif, where its extended aromatic framework aligned with exposed nucleobase surfaces. This orientation facilitates π–π stacking interactions, a key feature in the design of nucleic acid-targeting ligands, as such interactions enhance binding affinity through dispersion forces and stabilize secondary structures.

Detailed interaction analysis revealed that the ligand engages with both cytosine-rich regions and adjacent nucleobases within the cavity. Multiple hydrogen bonds (Table S3), with distances ranging from 1.95 to 3.64 Å, were observed between the ligand and residues including DC14, DC15, DC19, DG16, and DG21. In the context of drug design, hydrogen bonds are critical for conferring specificity and directional stability, and their presence suggests a well-defined binding orientation. Additionally, π–π stacking interactions with nucleobases further contribute to stabilization by anchoring the ligand within the cavity and restricting its conformational freedom.

The coexistence of hydrogen bonding, π–π stacking, and electrostatic interactions indicates a multivalent binding mechanism. Such multivalent interactions are highly desirable in rational drug design, as they enhance binding affinity while improving selectivity toward structured nucleic acid targets. The confined geometry of the i-motif cavity further restricts ligand mobility, favoring a single dominant binding mode rather than nonspecific surface association.

While docking provides a static representation of the binding pose, it serves as an essential first step in identifying key interaction hotspots and guiding subsequent optimization. The identification of residues such as DC14, DC15, DG16, and DG21 as primary interaction partners highlights potential targets for chemical modification in future ligand design. Functional groups capable of strengthening hydrogen bonding or π–π interactions at these positions could further enhance binding affinity and specificity.

Overall, the docking results suggest that the ligand is well accommodated within the i-motif cavity, forming a network of stabilizing interactions that are characteristic of effective nucleic acid-binding molecules. These findings provide a structural basis for subsequent molecular dynamics simulations and offer valuable insights for the rational design of next-generation i-motif stabilizers with potential therapeutic applications.

Molecular dynamics (MD) simulations were performed to validate the stability and characterize the binding mode of the ligand within the i-motif structure beyond static docking predictions. While molecular docking provides an initial estimate of binding affinity and pose, it inherently neglects conformational flexibility and solvent effects. Therefore, a 200 ns production MD simulation using the CHARMM36m force field was employed to evaluate the dynamic behavior of the ligand–i-motif complex under physiologically relevant conditions. Such simulations are essential in drug design to distinguish between kinetically trapped docking poses and thermodynamically stable binding modes.

The time evolution of the backbone RMSD indicated rapid equilibration within the first ~20 ns, followed by stabilization around ~0.45–0.50 nm, confirming the structural integrity of the i-motif throughout the simulation (Fig. S10a). In the context of drug design, this observation is critical, as excessive structural distortion of the nucleic acid scaffold upon ligand binding often correlates with nonspecific interactions or poor selectivity. The stable RMSD profile suggests that the ligand is accommodated without disrupting the native i-motif fold, an important criterion for selective targeting of nucleic acid secondary structures.

The ligand RMSD similarly plateaued after initial fluctuations, indicating that the ligand does not undergo large-scale translational or rotational diffusion (Fig. S10b). This behavior is indicative of confinement within a well-defined binding region rather than transient surface association. From a medicinal chemistry perspective, such restricted mobility reflects a favorable binding free energy landscape, where the ligand is energetically stabilized within a specific pocket, thereby increasing residence time,a key parameter associated with improved biological efficacy.

To explicitly characterize the binding site, residue-wise contact analysis (RMSF) was performed over the trajectory (Fig. S10c). Persistent interactions were observed with residues DC15, DG16, DG21, DC14, and DC19, confirming that the ligand remains localized within the central cavity region identified in docking. The identification of high-occupancy residues is particularly important for rational drug design, as these nucleobases constitute the “hotspot” region of binding. Targeting such hotspots enables the design of analogues with improved affinity and specificity through functional group optimization directed toward these residues.

Hydrogen bond analysis revealed an average of 4–5 stable hydrogen bonds during the simulation. In drug design, hydrogen bonds are critical determinants of specificity and directional binding (Fig. S10d). The persistence of these interactions indicates that the ligand forms a robust hydrogen-bonding network with the i-motif, contributing significantly to binding enthalpy. Moreover, the identification of high-occupancy hydrogen bonds provides actionable insight for lead optimization, as these interactions can be strengthened or replicated in derivative compounds.

In addition to hydrogen bonding, π–π stacking interactions between the ligand’s aromatic framework and nucleobase residues were maintained throughout the trajectory. Such interactions are particularly important in nucleic acid targeting, as they enhance binding through dispersion forces and contribute to the stabilization of secondary structures such as i-motifs. The coexistence of hydrogen bonding and π–π stacking suggests a multivalent interaction mechanism, which is often associated with high-affinity ligands and improved selectivity.

The radius of gyration (Rg) remained nearly constant (~1.10 nm), indicating that ligand binding does not perturb the global compactness of the i-motif (Fig. S10e). This observation is significant because effective i-motif stabilizers are expected to preserve or enhance the folded state rather than induce structural unfolding. Complementarily, RMSF analysis demonstrated reduced flexibility in residues lining the binding

pocket compared to distal regions, suggesting localized rigidification induced by ligand binding. Such rigidification is a hallmark of stabilizing ligands and is often correlated with increased structural persistence under physiological conditions.

Collectively, these findings demonstrate that the ligand adopts a stable and persistent binding mode within a confined cavity of the i-motif structure, stabilized by a synergistic combination of hydrogen bonding and π–π interactions. Importantly, the dynamic retention of key contacts, reduced flexibility of pocket residues, and absence of global structural disruption collectively support a structure-specific binding mechanism rather than nonspecific association. From a drug design standpoint, these results provide molecular-level validation that the ligand acts as a potential i-motif stabilizer, offering a promising scaffold for the development of nucleic acid-targeted therapeutics.

Table S3**.** Bond types and corresponding distances between the ligand **BPTC** and *h-TELO* i-motif

No.	Molecule Name ligand	Distance (Å)	Bond category	Bond type
1	:LIG:HN - :DC19:O3'	1.94928	Hydrogen Bond	Conventional Hydrogen Bond
2	:LIG:HC30 - :DC14:N3	2.39635	Hydrogen Bond	Carbon Hydrogen Bond
3	:LIG:HC16 - :DG16:O1P	2.57156	Hydrogen Bond	Carbon Hydrogen Bond
4	:LIG:HN1 - :DG3:O6	2.70560	Hydrogen Bond	Conventional Hydrogen Bond
5	:LIG:HC9 - :DG21:N7	2.88600	Hydrogen Bond	Carbon Hydrogen Bond
6	:LIG:HC6 - :DC15:O2	3.04765	Hydrogen Bond	Carbon Hydrogen Bond
7	:LIG:HC30 - :DG3:O6	3.06265	Hydrogen Bond	Carbon Hydrogen Bond
8	:LIG:HC11 - :DC19:O3'	3.06966	Hydrogen Bond	Carbon Hydrogen Bond
9	:DC15:H42 - :LIG	3.26576	Hydrogen Bond	Pi-Donor Hydrogen Bond
10	:DC1:O3' - :LIG	3.63951	Hydrogen Bond	Pi-Donor Hydrogen Bond
11	:LIG - :DG21	3.71729	Hydrophobic	Pi-Pi Stacked
12	:LIG:N4 - :DG21:O2P	4.49228	Electrostatic	Attractive Charge
13	:LIG:N4 - :DG16:O1P	4.58487	Electrostatic	Attractive Charge
14	:LIG - :DG21	4.66846	Hydrophobic	Pi-Pi Stacked
15	:LIG - :DC6	5.32127	Hydrophobic	Pi-Pi Stacked

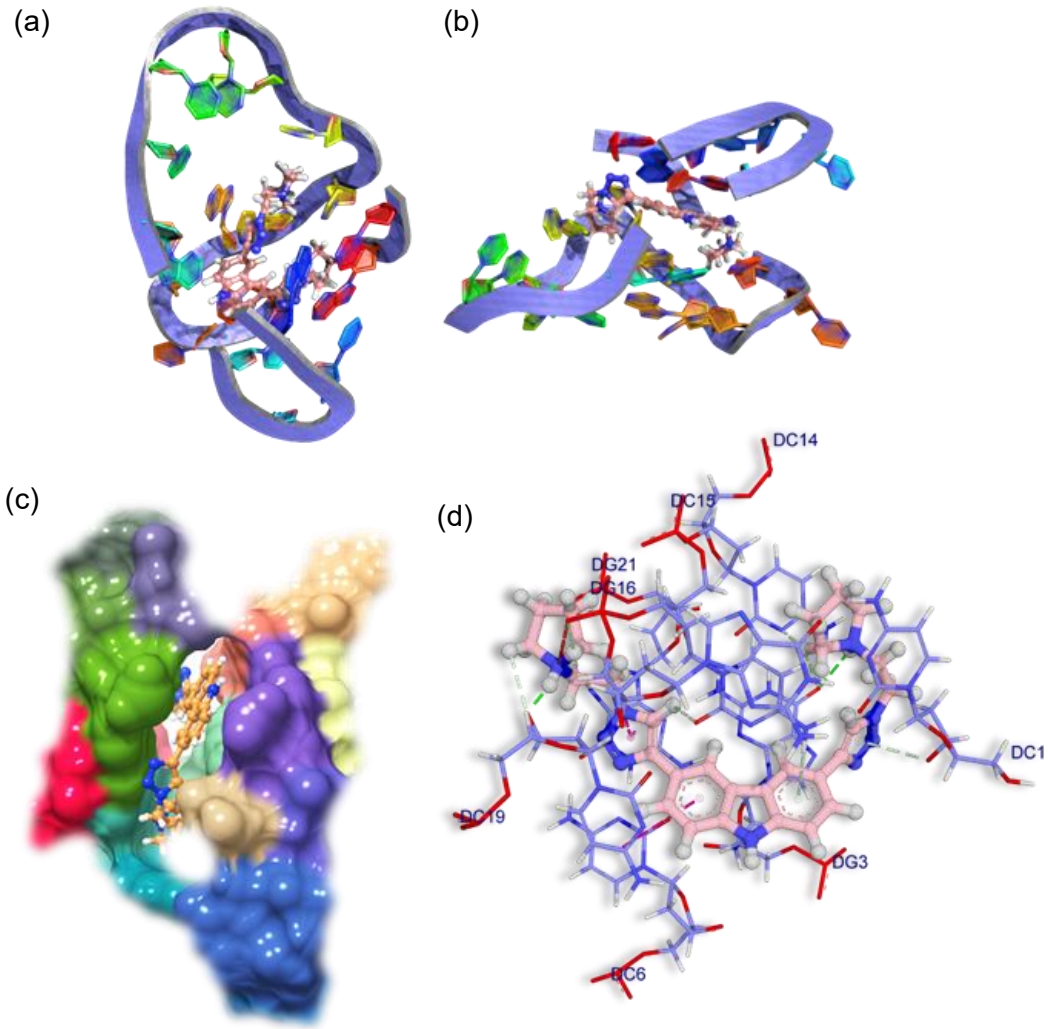

Fig. S9. Visualization of the i-motif–ligand complex following molecular docking. (a) the ligand (**BPTC**) is represented by pink ball and sticks, and the *h-TELO* i-motif structure (top view) is represented by cartoon (b) An alternative top view of the same figure. (c) The same complex is displayed with the *h-TELO* i-motif represented as a surface model, (d) Interaction map of the ligand with surrounding *h-TELO* i-motif base residues, where hydrogen bonds are shown as dotted lines and base residues involved in binding are labeled in blue two-letter nucleotide codes.

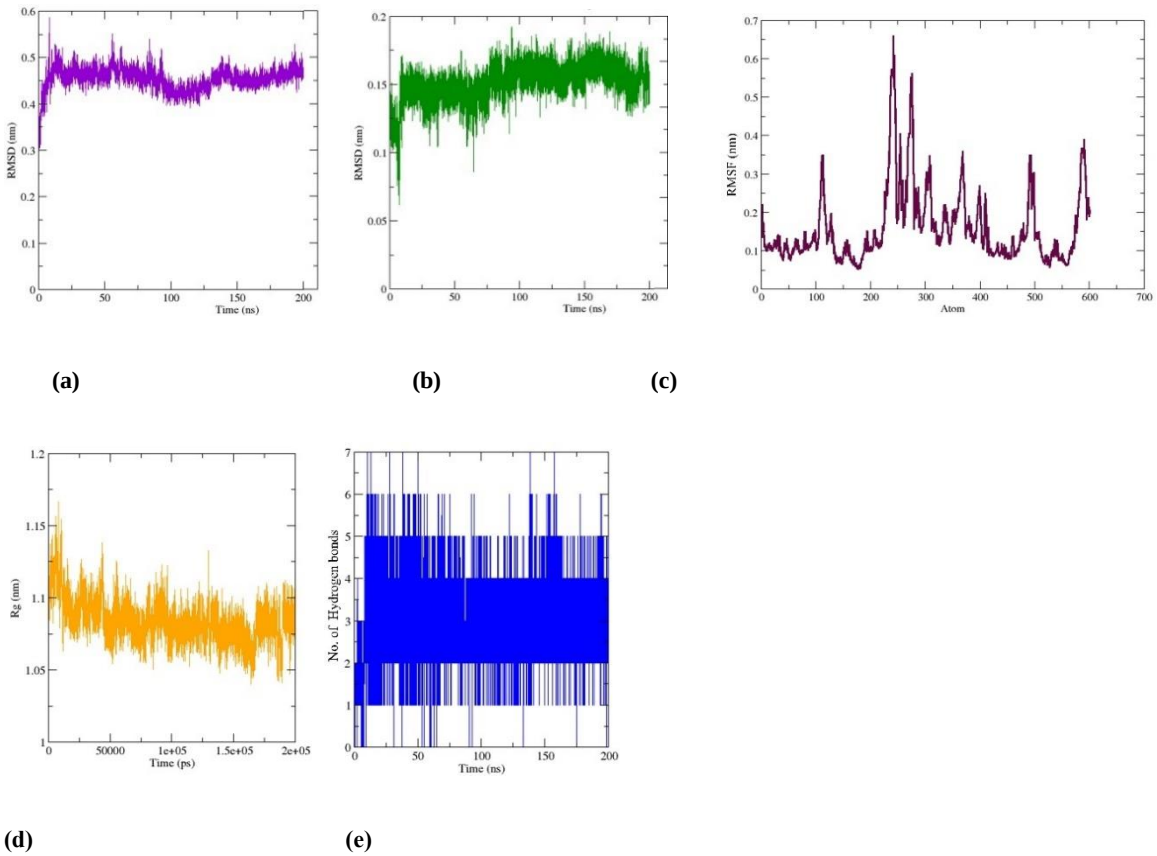

Fig. S10. (a) RMSD plot of i-motif–ligand complex during molecular dynamics simulation. (b) RMSD plot of ligand **BPTC**. (c) RMSF of the *h-TELO* i-motif during simulation with ligand. (d) Radius of gyration (Rg) plot of the *h-TELO* i-motif during simulation with ligand. (e) Number of H-bonds formed between the ligand **BPTC** and *h-TELO* i-motif over 200 ns.

14.0 Cell viability assay

To examine the cytotoxic property of **BPTC**, the XTT (2, 3-bis-(2- methoxy-4-nitro-5-sulfophenyl)-2H-tetrazolium-5-carboxanilide) assay was conducted in different cancer and normal cell lines. The experiments were carried out in triplicate on 96-well plates from lower (sub-micromolar) to higher (submilimolar) doses. Cells were grown (~ 10^5 cells/well) in 100 µL of culture medium and treated with increasing concentration of the compound **BPTC** (0 − 100 µM) followed by incubation for 24 h. The XTT/phenazine methosulfate (PMS) reagent was prepared by mixing 1 mg/mL of XTT in 3 mL of culture medium with subsequent addition of 7 µL of 10 mM PMS solution [dissolved in phosphate-buffered saline (PBS)]. This freshly prepared mixture solution (25 µL) was then directly added to each well and incubated for 2 h at 37 °C. The absorbance values of XTT formazan were measured at 450 nm on a Multiskan FC microplate spectrophotometer (Thermo Scientific). The calculation of cell growth percentage was done using the below equation: % of cell viability = (OD of treated cells/OD of untreated control cells) x 100.

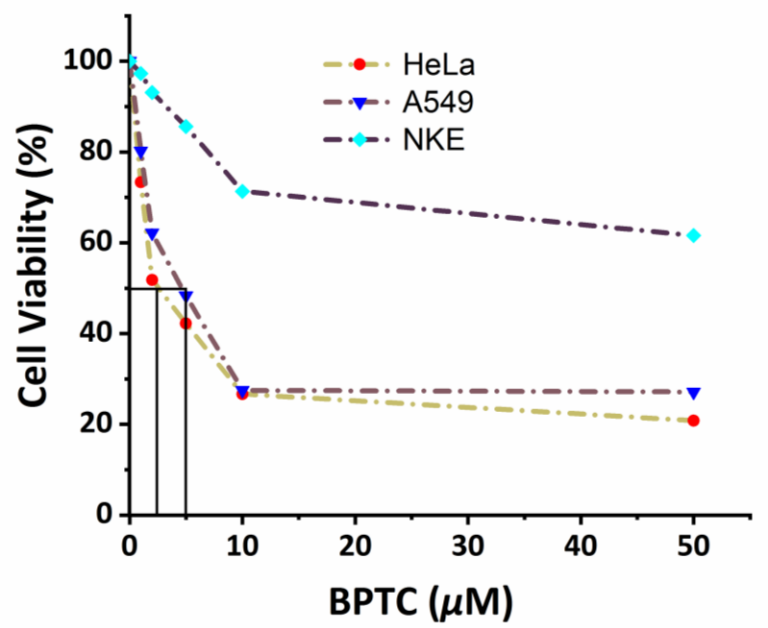

Fig. S11. Cell viability measurement of **BPTC** in HeLa (cervical cancer), A549 (lung carcinoma) and NKE (normal kidney epithelial) cell lines.

15.0 Cell cycle assay

Hela cells were seeded in six-well plates at a density of 1×10^6 cells per well and incubated for 24 h prior to treatment. Then, cells were treated with 1 µM and 2 µM **BPTC** for 24 h. Following treatment, cells were harvested and fixed using 2 mL of ice-cold 70% ethanol, followed by overnight incubation at 4 °C. Fixed cells were pelleted and resuspended in 350 µL PBS containing 0.2 µg/mL RNase A (Invitrogen) and 5 µL of 1 mg/mL propidium iodide (PI), followed by incubation at 37 °C for 30 min in the dark. Cell cycle distribution was analyzed by flow cytometry (BD Biosciences), with a minimum of 10,000 events recorded per sample.

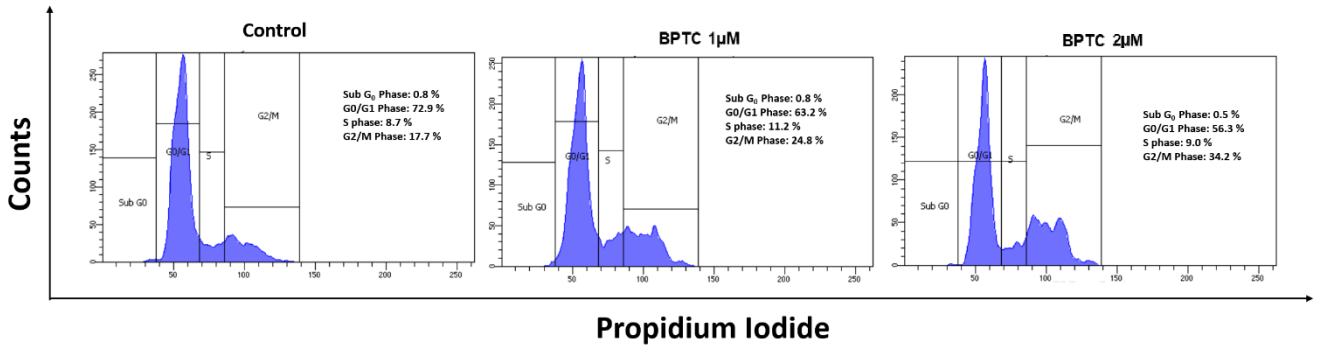

Fig. S12. Flow cytometric analysis of HeLa cells treated with **BPTC**. Cell cycle distribution of HeLa cells following 24 h treatment with **BPTC** at 1 µM and 2 µM, respectively.

16.0 Apoptosis assay

Hela cells were seeded in six-well plates at a density of 1 × 10^6 cells/mL and incubated overnight at 37 °C. Cells were then treated with 1 µM and 2 µM **BPTC** for 24 h while untreated cells were kept as the experimental control. Following treatment, cells were trypsinized, washed twice with cold PBS, and centrifuged at 1800 rpm for 5 min. The cell pellets were resuspended in 350 µL of 1× Annexin V binding buffer (10 mM HEPES, pH 7.4, 140 mM NaCl, 2.5 mM $CaCl_2$), followed by the addition of 5 µL Annexin V-FITC and 1 µL propidium iodide (1 mg/mL). Samples were incubated on ice for 5 min and immediately analyzed by flow cytometry (BD Biosciences). A minimum of 10,000 events were recorded per sample.

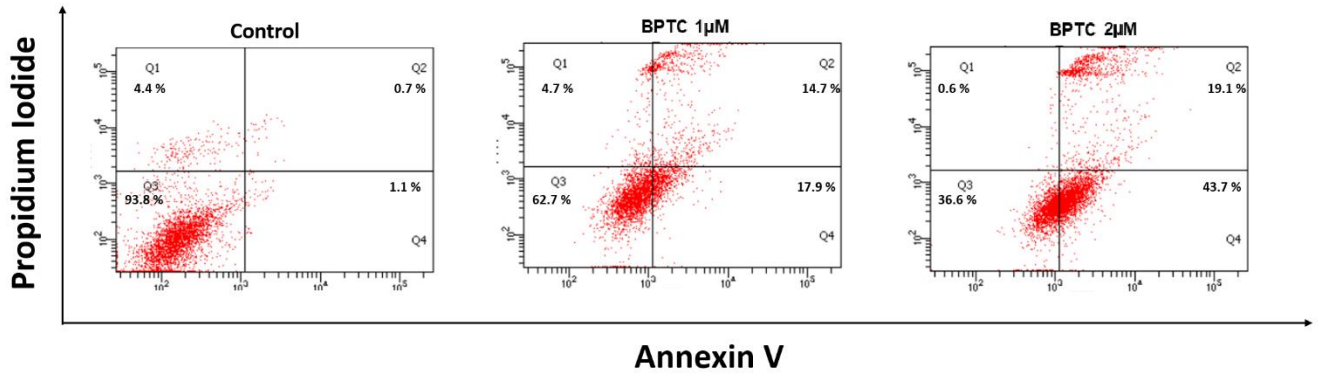

Fig. S13. Apoptosis analysis of HeLa cells with **BPTC** at 1 µM and 2 µM, respectively, assessed using annexin V/PI staining.

17.0 Telomerase repeat amplification protocol (TRAP)

HeLa cells were treated with **BPTC**, and telomerase activity was assessed using the Q-TRAP assay with the TRAPeze Telomerase Detection Kit (Merck). Cells were lysed in CHAPS buffer, and supernatants were collected after centrifugation. Telomerase extension was performed using 5 µg of protein extract in TRAP buffer with TS primer, dNTPs, and **BPTC**. Heat-inactivated extracts served as negative controls. Extended products were purified via phenol/chloroform extraction, ethanol-precipitated, and resuspended in PCR-grade water. qPCR was performed using SYBR Green. Relative telomerase activity (RTA) was calculated from a standard curve of untreated extracts using the formula:

RTA = 10^[(Ct_sample – m)/slope]. Data were analyzed in OriginPro 2018.

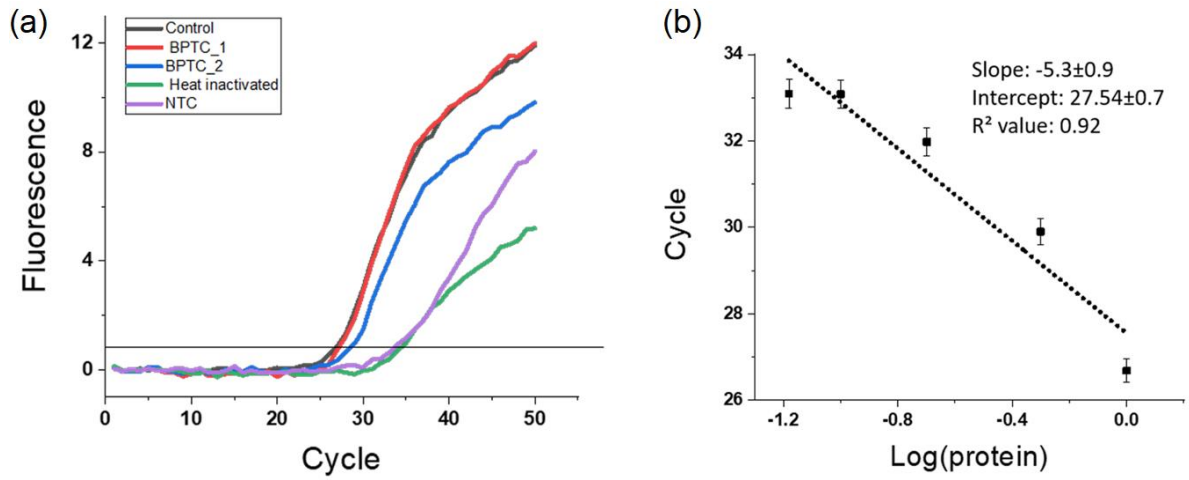

Fig. S14. (a) qPCR amplification curves from Q-TRAP assay for quantification of telomerase activity in HeLa cells treated with **BPTC** (b) Standard curve for quantification of telomerase activity in the Q-TRAP assay.

18.0 References:

[1] P. Saha, D. Panda, D. Müller, A. Maity, H. Schwalbe and J. Dash, *Chem. Sci.*, 2020, **11**, 2058.
[2] Z. P. Demko and K. B. Sharpless, *Org. Lett.*, 2001, **3**, 4091–4094.
[3] H. W. El-Shafey, R. M. Gomaa, S. M. El-Messery and F. E. Goda, *Bioorg. Chem.*, 2020, **101**, 103987.
[4] J. M. Smith, J. R. Frost and R. Fasan, *Chem. Commun.*, 2014, **50**, 5027–5030.
[5] P. S. Rao, C. Kurumurthy, B. Veeraswamy, G. Santhosh Kumar, Y. Poornachandra, C. Ganesh Kumar, S. B. Vasamsetti, S. Kotamraju and B. Narsaiah, *Eur. J. Med. Chem.*, 2014, **80**, 184–191.
[6] H. Yan, P. Yue, Z. F. Li, Z. F. Guo, Z. L. Lu, *Sci. China Chem.*, 2014, **57**, 296–306.
[7] J. Hannant, J. H. Hedley, J. Pate, A. Walli, S. A. F. Al-Said, M. A. Galindo, B. A. Connolly, B. R. Horrocks, A. Houlton and A. R. Pike, *Chem. Commun.*, 2010, **46**, 5870–5872.
[8] Y.-L. Yang, Y.-P. Lee, Y.-L. Yang and P.-C. Lin, *ACS Chem. Biol.*, 2014, **9**, 390–397.
[9] M. Debnath, S. Ghosh, D. Panda, I. Bessi, H. Schwalbe, K. Bhattacharyya and J. Dash, *Chem. Sci.*, 2016, **7**, 3279–3285.
[10] L. Xu, S. Hong, N. Sun, K. Wang, L. Zhou, L. Ji and R. Pei, *Chem. Commun.*, 2016, **52**, 179–182.
[11] Q. Sheng, J. C. Neaverson, T. Mahmoud, C. E. M. Stevenson, S. E. Matthews and Z. A. E. Waller, *Org. Biomol. Chem.*, 2017, **15**, 5669–5673.
[12] M. Debnath, S. Ghosh, A. Chauhan, R. Paul, K. Bhattacharyya and J. Dash, *Chem. Sci.*, 2017, **8**, 7448–7456.
[13] D. Müller, P. Saha, D. Panda, J. Dash and H. Schwalbe, *Chem. Eur. J.*, 2021, **27**, 12726–12736.
[14] X. Li, J. Wang, X. Gong, M. Zhang, S. Kang, B. Shu, Z.-S. Huang, D. Li, *Nucleic Acids Res.*, 2020, **48**, 8255–8268.
[15] S. Kendrick, H.-J. Kang, M. P. Alam, M. M. Madathil, P. Agrawal, V. Gokhale, D. Yang, S. M. Hecht and L. H. Hurley, *J. Am. Chem. Soc.*, 2014, **136**, 4161–4171.
[16] G. Kuang, M. Zhang, S. Kang, D. Hu, X. Li, Z. Wei, X. Gong, L.-K. An, Z.-S. Huang, B. Shu, D. Li, *J. Med. Chem.*, 2020, **63**, 9136–9153.
[17] Y. P. Kumar, P. Saha, D. Saha, I. Bessi, H. Schwalbe, S. Chowdhury and J. Dash, *ChemBioChem*, 2016, **17**, 388–393.
[18] Z. Niknezhad, L. Hassani and D. Norouzi, *Mater. Sci. Eng. C*, 2016, **58**, 1188–1193.
[19] S. N. Journey, S. L. Alden, W. M. Hewitt, M. L. Peach, M. C. Nicklaus, J. S. Schneekloth Jr., *MedChemComm*, 2018, **9**, 2000–2007.
[20] S. Takahashi, S. Bhattacharjee, S. Ghosh, N. Sugimoto and S. Bhowmik, *Sci. Rep.*, 2020, **10**, 2504.
[21] H. Xu, H. Zhang and X. Qu, *J. Inorg. Biochem.*, 2006, **100**, 1646–1652.
[22] N. Gao, Y. Wang and C. Wei, *Chem. Res. Chin. Univ.*, 2014, **30**, 495–499.
[23] D.-L. Ma, M. H.-T. Kwan, D. S.-H. Chan, P. Lee, H. Yang, V. P. Y. Ma, L. P. Bai, Z.-H. Jiang and C.-H. Leung, *Analyst*, 2011, **136**, 2692–2696.
[24] P. Spence, J. Fielden and Z. A. E. Waller, *J. Am. Chem. Soc.*, 2020, **142**, 13856–13866.
[25] M. M. Molnar, S. C. Liddell, R. M. Wadkins, *ACS Omega*, 2019, **4**, 8967–8973.
[26] S. Satpathi, S. Sappati, K. Das and P. Hazra, *Org. Biomol. Chem.*, 2019, **17**, 5392–5399.

[27] B. Mir, I. Serrano-Chacón, P. Medina, V. Macaluso, M. Terrazas, A. Gandioso, M. Garavís, M. Orozco, N. Escaja and C. González, *Nucleic Acids Res.*, 2024, **52**, 3375–3389.
[28] H. Abou Assi, M. Garavís, C. González and M. J. Damha, *Nucleic Acids Res.*, 2018, **46**, 8038–8056.
[29] X. Luo, J. Zhang, Y. Gao, W. Pan, Y. Yang, X. Li, L. Chen, C. Wang and Y. Wang, *Front. Pharmacol.*, 2023, **14**, 1136251.
[30] F. A. Kolpakov and V. N. Babenko, *Mol. Biol.*, 1997, **31**, 540-547.
[31] O. Trott and A. J. Olson, *J. Comput. Chem.*, 2010, **31**, 455-461.
[32] C. L. Brooks III and M. Karplus, *J. Mol. Biol.*, 1989, **208**, 159-181.
[33] V. Zoete, M. A. Cuendet, A. Grosdidier and O. Michielin, *J. Comput. Chem.*, 2011, **32**, 2359-2368.
[34] T. Darden, D. York and L. Pedersen, *J. Chem. Phys.*, 1993, **98**, 10089-92.
[35] J. Dash, P. S. Shirude, S.-T. D. Hsu and S. Balasubramanian, *J. Am. Chem. Soc.*, 2008, **130**, 15950–15956.
[36] I. Bessi, H. R. A. Jonker, C. Richter and H. Schwalbe, *Angew. Chem., Int. Ed.*, 2015, **54**, 8444–8448.
[37] S. Kendrick, H.-J. Kang, M. P. Alam, M. M. Madathil, P. Agrawal, V. Gokhale, D. Yang, S. M. Hecht and L. H. Hurley, *J. Am. Chem. Soc.*, 2014, **136**, 4161–4171.
[38] Z. A. E. Waller, S. A. Sewitz, S.-T. D. Hsu and S. Balasubramanian, *J. Am. Chem. Soc.*, 2009, **131**, 12628–12633.
[39] S. Neidle, *Nat. Rev. Chem.*, 2017, **1**, 0041.